

Phantom scalar-tensor models and cosmological tensions

Mario Ballardini,^{1,2,3} Angelo G. Ferrari,^{4,5} Fabio Finelli^{3,5}

¹Dipartimento di Fisica e Scienze della Terra, Università degli Studi di Ferrara, via Giuseppe Saragat 1, 44122 Ferrara, Italy

²INFN, Sezione di Ferrara, via Giuseppe Saragat 1, 44122 Ferrara, Italy

³INAF/OAS Bologna, via Piero Gobetti 101, 40129 Bologna, Italy

⁴Dipartimento di Fisica e Astronomia, Università di Bologna, viale Berti Pichat 6/2, 40127 Bologna, Italy

⁵INFN, Sezione di Bologna, viale C. Berti Pichat 6/2, 40127 Bologna, Italy

E-mail: mario.ballardini@unife.it, angelo.ferrari3@unibo.it,
fabio.finelli@inaf.it

Abstract. We study three different extended scalar-tensor theories of gravity by also allowing a negative sign for the kinetic term for the scalar field in the Jordan frame. Our scope is to understand how the observational constraints for these models cope with the volume of the parameter space in which the theory is healthy. Models with a negative kinetic term lead to decreasing effective gravitational constant with redshift and behave as an effective relativistic component with a negative energy density as opposite to their corresponding version with a standard kinetic term. As a consequence, we find that the extended branch with a negative sign for the kinetic term correspond in general to lower H_0 and σ_8 compared to Λ CDM. We find that in all the cases with a negative sign for the kinetic term studied here, cosmological observations constrain these models around GR and prefer a volume of the parameter space in which the theory is not healthy since the scalar field behave as a ghost also in the related Einstein frame. We show that also in the phantom branch early modify gravity with a quartic coupling can substantially reduce the H_0 tension fitting the combination of cosmic microwave background data from *Planck*, baryon acoustic oscillations from BOSS and eBOSS, and Supernovae from the Pantheon sample with calibration information by SHOES.

Contents

1	Introduction	1
2	Theory and cosmological background dynamics	3
3	Constraints and results	4
3.1	Phantom induced gravity	5
3.2	Phantom non-minimal coupling	12
3.3	Phantom early modified gravity	12
4	Conclusions	15
A	Tables	18
B	Background equations	20
C	Linear perturbed equations	22
C.1	The perturbed Einstein field equations	22
C.2	The perturbed Klein-Gordon equation	24
D	Initial conditions	24
E	Comparison between BAO, and FS + BAO joint analysis	25

1 Introduction

The Λ CDM model represents the current standard cosmological model providing an excellent fit to most of cosmological observations: measurements of luminosity distances of Type Ia Supernovae (SN Ia) [1–3], measurements of cosmic microwave background (CMB) anisotropies in temperature and polarization [4], measurements of the baryon acoustic oscillations (BAO) in galaxy and cluster distribution [5, 6], cosmic shear measurements of the CMB [7–9] and of the galaxy distribution [10, 11], and the predicted abundance of light elements [12]. While the Λ CDM model provides an accurate description to most of cosmological observations, it relies on a number of assumptions and unknown ingredients such dark matter, dark energy, and a suitable mechanism to produce its initial condition.

In addition to the interest in testing at which extent the validity of the Λ CDM model holds with better and more data, the theoretical search for extended models [13–21] has been fueled by the persisting cosmological tensions or rather intriguing inconsistencies between different measurements under the framework of the minimal Λ CDM model; see Refs. [22–29] for reviews on the topic.

Among the many proposed models, there are still difficulties in finding a candidate able to completely solve the discrepancy between the value of the Hubble parameter inferred in Λ CDM using CMB data from the *Planck* DR3, i.e. $H_0 = (67.36 \pm 0.54) \text{ km s}^{-1} \text{ Mpc}^{-1}$ at 68% confidence level (CL) [30], with the measurement from the SH0ES team [31] obtained with cosmic distance ladder calibration of SN Ia from the revised Pantheon+ compilation [3], i.e. $H_0 = (73.0 \pm 1.0) \text{ km s}^{-1} \text{ Mpc}^{-1}$ at 68% CL, once all cosmological data are combined.

It is even more difficult to reconcile the value of the Hubble parameter together with the persistent but less significant tension between *Planck* and galaxy shear experiments, quantified through the value of $S_8 \equiv \sigma_8 \sqrt{\Omega_m}/0.3$, see [27]. Adopting a flat Λ CDM model, cosmic shear analysis of the fourth data release of the *Kilo-Degree Survey* (KiDS-1000) reported $S_8 = 0.759^{+0.024}_{-0.021}$ [10] and $S_8 = 0.776 \pm 0.017$ from *Dark Energy Survey* (DES) Year 3 (Y3) combination of three large-scale structures (LSS) two-point correlation functions (3×2 pt) [11], while the value measured by *Planck* corresponds to $S_8 = 0.832 \pm 0.013$ [30]. Indeed, while minimally and nonminimally coupled scalar field have been extensively studied as possible solutions to the Hubble tension, they usually lead to a higher value of the Hubble constant together with a larger growth of structures on small scales, i.e. a higher value of σ_8 , see Refs. [13, 14, 32–36]. However, they generally predict a value of S_8 compatible to the one obtained in Λ CDM avoiding to exacerbate the tension on the growth of structure amplitude since the larger σ_8 is compensated by a larger value of H_0 and a lower value of Ω_m [20, 37–39].

One possibility is to extend the dynamics of the scalar field to behave differently at early- and late-time in order to solve both tensions at the same time. The possibility to have models with phenomenology in both the early and late universe has been tried in the context of modified gravity [20, 38], early dark sector [40], and combining modified gravity or early dark energy to extended neutrino physics [19, 41, 42].

In this paper, we study modified gravity models with a nonminimally coupled scalar field with negative kinetic energy, so-called *phantom* field. Note that this is not strictly related to the phantom dark energy models for which the dark energy (DE) equation of state can cross the *phantom divide* line $w_{\text{DE}} = -1$. Moreover, scalar-tensor models can be realized with no necessity to introduce a ghost field [43] avoiding the problems in ghost phantom DE [44] to be plagued by classical and quantum instabilities [45]. Such a non-canonical kinetic energy term can occur in supergravity models [46] and in higher derivative theories of gravity [47]. We show how a nonminimally coupled scalar field with the negative sign of its kinetic term (phantom branch) behaves differently compared to the case with standard kinetic term (standard branch) and we derive the constraints on these models combining the information from *Planck* 2018 DR3 CMB temperature, polarization and lensing, together with a compilation of BAO measurements from the releases DR7 and DR12 of the *Baryon Oscillation Spectroscopic Survey* (BOSS) and Ly α measurements from the *extended Baryon Oscillation Spectroscopic Survey* (eBOSS), and uncalibrated SN Ia from the Pantheon sample.

The paper is organized as follows. After this introduction, we describe the implementation of the various basic quantities in the context of scalar-tensor theories in Section 2. In Section 3, we describe the datasets and prior considered and we discuss

our results for the three models studied: induced gravity, non-minimal coupling, and early modified gravity. In Section 4 we draw our conclusions. In Appendix A, we collect the tables with the constraints on all the cosmological parameters obtained with our MCMC analysis. Background equations, linear perturbations, and initial conditions for background and cosmological fluctuations are collected in Appendices B-C-D. In Appendix E, we present a comparison of the results by using CMB data plus different combinations of LSS measurements.

2 Theory and cosmological background dynamics

We study the action for the scalar-tensor theory in Jordan frame [48] which is given by

$$\mathcal{S} = \int d^4x \sqrt{|g|} \left[\frac{F(\sigma)R}{2} - \frac{Z(\sigma)}{2}(\partial\sigma)^2 - V(\sigma) + \mathcal{L}_m \right] \quad (2.1)$$

where $|g|$ is the absolute value of the determinant of the metric $g_{\mu\nu}$, σ is the scalar field, $F(\sigma)$ is the non-minimal coupling function, R is the Ricci scalar, $V(\sigma)$ is the potential for σ , and \mathcal{L}_m the Lagrangian density of matter minimally coupled to the metric (without introducing any direct coupling between the scalar field and the matter content we guarantee that the weak equivalence principle is exactly satisfied). The function $Z(\sigma)$ in front of the kinetic term can be set to ± 1 by a redefinition of the scalar field.

In this model, the effective gravitational constant G_{eff} for the attraction between two test masses [having the same physical meaning as the Newton gravitational constant in general relativity (GR)] is given by

$$G_{\text{eff}} = \frac{1}{8\pi F} \frac{ZF + 2F_\sigma^2}{ZF + \frac{3}{2}F_\sigma^2} \quad (2.2)$$

on all scales for which the scalar field is effectively massless [43], i.e. $V_\sigma \simeq 0$ and $V_{\sigma\sigma} \simeq 0$.

The current values of the time derivative and field derivative of coupling F in these theories - assuming a homogeneous evolution of the scalar field for all the scales - are strongly constrained by Solar System tests of post-Newtonian parameters (for these quantities, we drop here the subscript 0)

$$\gamma_{\text{PN}} = 1 - \frac{F_\sigma^2}{ZF + 2F_\sigma^2} \quad (2.3)$$

$$\beta_{\text{PN}} = 1 + \frac{1}{4} \frac{FF_\sigma}{2ZF + 3F_\sigma^2} \frac{d\gamma_{\text{PN}}}{d\sigma} \quad (2.4)$$

as well as the time variation of the effective cosmological constant. Current constraints [49–52] correspond to

$$\gamma_{\text{PN}} - 1 = (2.1 \pm 2.3) \cdot 10^{-5} \quad (2.5)$$

$$\beta_{\text{PN}} - 1 = (-4.1 \pm 7.8) \cdot 10^{-4} \quad (2.6)$$

$$\dot{G}/G = (7.1 \pm 7.6) \cdot 10^{-14} \text{ yr}^{-1}. \quad (2.7)$$

On cosmological scales, post-Newtonian parameters are weakly constrained from current cosmological data, see Ref. [19], with the perspective to reach the Solar System accuracy with the combination of future cosmological surveys [38, 53, 54].

There are essentially two stability conditions which impact on these scalar-tensor theories. The condition

$$G_{\text{eff}} > 0 \tag{2.8}$$

is one of the stability conditions of this theory meaning that the graviton is not a ghost. Moreover, we have the inequality

$$\frac{ZF}{F_\sigma^2} > -\frac{3}{2} \tag{2.9}$$

requiring the positivity of the kinetic energy of the scalar field in the Einstein frame [55]. Eqs. (2.8)-(2.9) reduce to $ZFF_\sigma^{-2} > 0$ for $Z = +1$ or $-3/2 < ZFF_\sigma^{-2} < 0$ for $Z = -1$, and to $F > 0$. This condition can be mapped to a range of allowed parameter space for the parameters modelling $F(\sigma)$. However, we will consider a larger parameter space in the following analysis testing the models also for parameters violating the stability conditions in an agnostic way.

3 Constraints and results

In this section, we present our constraints on the cosmological parameters of the models studied. In particular, we study the nonminimally coupling $F = \xi\sigma^2$, i.e. *induced gravity* (IG) [56, 57], and $F = N_{\text{pl}}^2 + \xi\sigma^2$ (hereafter NMC) both with a phantom scalar field, i.e. $Z = -1$; in both cases we consider $V(\sigma) = \lambda F^2(\sigma)/4$ which yields to an effectively massless dynamic [58, 59]. We study also the *early modified gravity* (EMG) model proposed in Ref. [20] extended to $Z = -1$. This last case is given by $F = M_{\text{pl}}^2 + \xi\sigma^2$ and $V = \Lambda + \lambda\sigma^4/4$ with a negative amplitude λ of the self-interaction term in order to produce the peculiar evolution of the scalar field damped into coherent oscillations within the phantom branch. We perform a Markov-chain Monte Carlo (MCMC) analysis using a modified version of the CLASSig code [13], based on the Einstein-Boltzmann code CLASS¹ [60, 61], interfaced to the publicly sampling code MontePython² [62, 63]. The datasets used in this work include

- P18 refers to the CMB temperature, polarization, and lensing from *Planck* DR3 [64, 65].
- FS refers to the combination of pre-reconstructed full-shape monopole and quadrupole galaxy power spectra for three different sky-cuts CMASS NGC, CMASS SGC and LOWZ NGC [66] based on the publicly available code PyBird³[67].

¹https://github.com/lesgourg/class_public

²https://github.com/brinckmann/montepython_public

³<https://github.com/pierrexyz/pybird/>

- BAO refers to the post-reconstruction measurements from BOSS DR12 [68], low- z BAO measurements from SDSS DR7 6dF and MGS [69, 70], Ly α BAO measurements from eBOSS, and combination of those [71–73].
- SN refers to the Pantheon catalogue of high-redshift supernovae, spanning the redshift range $0.01 < z < 2.3$ [74]⁴.
- Additional constraints of a Gaussian prior on the density of baryons (hereafter BBN) motivated from Big Bang nucleosynthesis (BBN) constraints corresponding to $\omega_b = 0.02235 \pm 0.0005$ [12], used in combination to FS and SN for the CMB-independent analysis.
- Additional constraints that include a Gaussian prior on the Hubble constant [hereafter $p(H_0)$], $H_0 = (73.04 \pm 1.04) \text{ km s}^{-1} \text{ Mpc}^{-1}$ at 68% CL, from Ref. [31].

We vary 6 standard parameters, i.e. ω_b , ω_c , H_0 , τ , $\ln(10^{10} A_s)$, n_s , and the modified gravity parameters. We assume 2 massless neutrino with $N_{\text{nr}} = 2.0328$, and a massive one with fixed minimum mass $m_\nu = 0.06 \text{ eV}$. We fix the primordial ^4He mass fraction Y_p according to the prediction from PArthENoPE [75, 76], by taking into account the relation with the baryon fraction ω_b and the varying gravitational constant which enters in the Friedman equation during nucleosynthesis.

Following the minimization method of Ref. [27], we report for each combination of datasets the $\Delta\chi^2$ values calculated with respect to the ΛCDM model where negative values correspond to a better fit of the dataset.

3.1 Phantom induced gravity

For IG (or equivalently extended Jordan-Brans-Dicke), with coupling $F(\sigma) = \xi\sigma^2$, we sample on the quantity $\zeta_{\text{IG}} \equiv \ln(1 + 4\xi)$ which corresponds to a linear prior on the coupling to the parameter ξ for $\xi \ll 1$. Here we impose the following boundary condition on the current value of the effective gravitational constant

$$G_{\text{eff}}(z = 0) = G \quad (3.1)$$

which fixes the final value of the scalar field.

Scalar-tensor theories of gravity such as extended Jordan-Brans-Dicke models, lead to a modification of the Hubble parameter H_0 due to the time evolution of σ and due to the redshift evolution of the gravitational strength. Indeed, a variation of the strength of gravity can be connected to a change of the expansion rate of the universe as

$$\frac{H(\xi \neq 0)}{H(\xi = 0)} \approx \frac{M_{\text{Pl}}^2}{F(\sigma)}. \quad (3.2)$$

For a fixed matter content, reducing the Planck mass $F(\sigma) < M_{\text{Pl}}^2$ with respect to the GR prediction increases the expansion rate at a given time and consequently reduces

⁴<https://github.com/dscolnic/Pantheon>

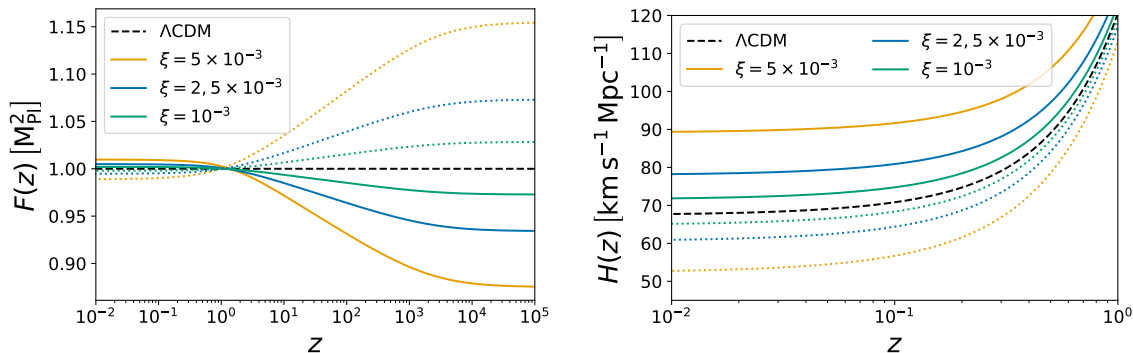


Figure 1. Time evolution of the coupling to the Ricci scalar $F = \xi\sigma^2$ (left panel) and of the Hubble parameter (right panel) for different values of the coupling parameter ξ in the standard branch (solid lines) and in the phantom one (dashed lines) for IG ($F = \xi\sigma^2$, $V = \lambda F^2/4$).

the comoving sound horizon at recombination

$$r_s = \int_{z_*}^{\infty} dz' \frac{c_s(z')}{H(z')} \quad (3.3)$$

where z_* is the redshift parameter at recombination and c_s is the speed of sound in the photon-baryon fluid. We show in Fig. 1 that the coupling function increases in the branch with standard kinetic term (solid lines) while decreasing in the phantom branch (dashed lines). This different behaviour is connected with a different late-time evolution of the Hubble parameter (when the scalar field starts to evolve driven by the non-relativistic matter) which is larger than the Λ CDM case in the standard branch and lower in the phantom branch. This effect induces also a modification on the comoving angular diameter distance

$$D_M(z) = \int_0^z \frac{dz'}{H(z')} \quad (3.4)$$

and does not cancel out on the angular size of horizon at the last-scattering surface θ_*

$$\theta_* = \frac{r_s}{D_M(z_*)} \quad (3.5)$$

driving a shift on the acoustic peaks of the CMB connected to the evolution of the coupling F [19, 77, 78]. In Fig. 2, we show the shift of the acoustic peaks of the CMB temperature anisotropies angular power spectrum imprinted by the evolving effective Planck mass. The peaks move to the right in the positive branch and to the left in the phantom one. Indeed, in order to compensate this shift (keeping nearly unchanged the value of the CDM density parameter) the two branches go in the direction of a larger or a smaller value of Ω_m once the CMB data are included in the analysis, see Fig. 3. Therefore it is possible to break the degeneracy at background level between the scalar field σ and the density parameters by combining early- and late-time probes.

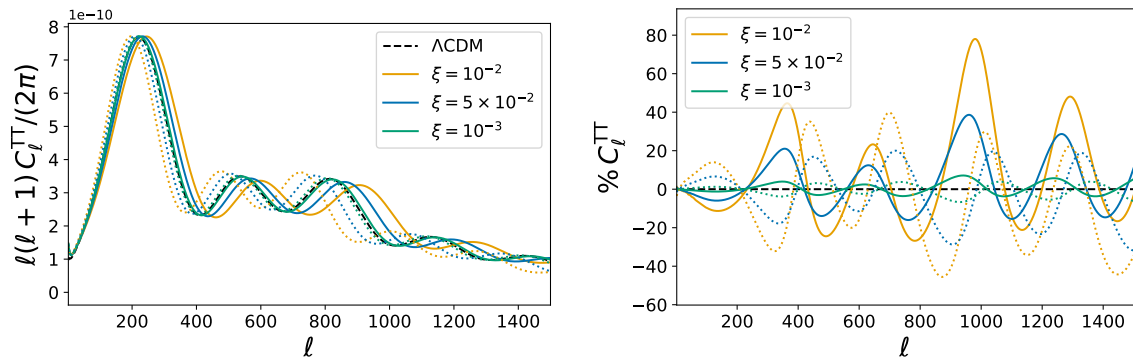


Figure 2. CMB temperature anisotropies power spectrum (left panel) and relative differences with respect to the Λ CDM case (right panel) for different values of the coupling parameter ξ in the standard branch (solid lines) and in the phantom one (dashed lines) for IG ($F = \xi\sigma^2$, $V = \lambda F^2/4$).

In Fig. 3, we compare the CMB-only constraints for IG in the phantom branch to the standard case. We see that the degeneracy direction in the ξ - H_0 plane changes orientation going from one case to the other according to Eq. (3.2). It turns out that the phantom branch allows much larger values of the coupling ξ and predicts a lower value for the Hubble constant without any prospect to reduce the H_0 tension. It is interesting to note that the extension of our study to the phantom case strengthens the correspondence between the kinetic term and the spatial curvature: the standard (phantom) kinetic term shifts the position to the right (left) as a negative (positive) spatial curvature.

Finally, it is interesting to note that the matter density root mean square fluctuations σ_8 goes toward lower values in the phantom branch compared to both the standard branch and the Λ CDM model predictions, see Fig. 5. This behaviour can be understood studying the late-time solution of the perturbation equation for the matter density contrast in the linear regime, on sub-horizon scales

$$\delta_m'' + \left(\frac{3}{a} + \frac{H'}{H}\right) \delta_m' - \frac{G_{\text{eff}}}{2GH^2} \frac{\rho_m}{a^2} \delta_m \simeq 0 \quad (3.6)$$

where primes are derivatives with respect to the scale factor a . By rewriting the Friedmann equations (B.4)-(B.5)

$$H^2 = \frac{\rho + V}{3F(1+f)} \quad (3.7)$$

$$\frac{H'}{H} = -\frac{3}{2a} - \frac{3}{a}w - \frac{F'}{2F} + \frac{f'}{2} \quad (3.8)$$

introducing the quantity

$$f = -a \frac{F_\sigma}{F} \sigma' - \frac{a^2 Z}{6F} \sigma'^2 \quad (3.9)$$

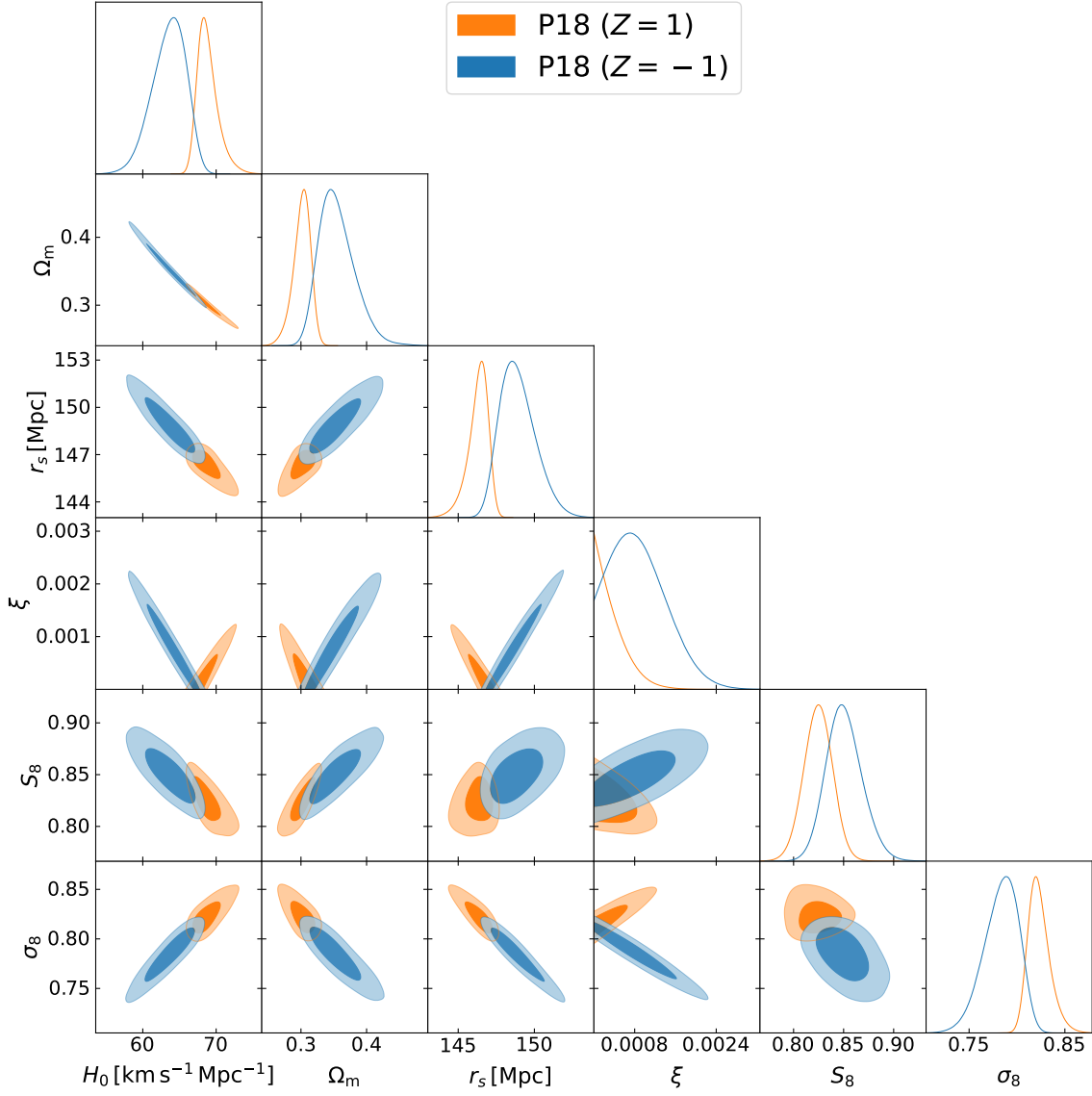


Figure 3. Marginalized joint 68% and 95% CL regions 2D parameter space using the CMB alone data for IG ($F = \xi\sigma^2$, $V = \lambda F^2/4$) with $Z = 1$ (orange) and for IG with $Z = -1$ (blue).

and where we used $\rho'/\rho = -3(1+w)/a$, we can write Eq. (3.6) as

$$\delta_m'' + \left[\frac{3}{2a}(1-w) - \frac{F'}{2F} + \frac{f'}{2} \right] \delta_m' - \frac{3}{2a^2} \frac{2ZF + 4F_\sigma^2}{2ZF + 3F_\sigma^2} (1-f) \frac{\rho_m}{\rho + V} \delta_m \simeq 0. \quad (3.10)$$

During the matter-dominated era, the scalar field evolves as $\sigma \sim a^{2Z\xi}$ [59] leading for IG to

$$f \sim -\frac{10Z\xi}{3} \quad (3.11)$$

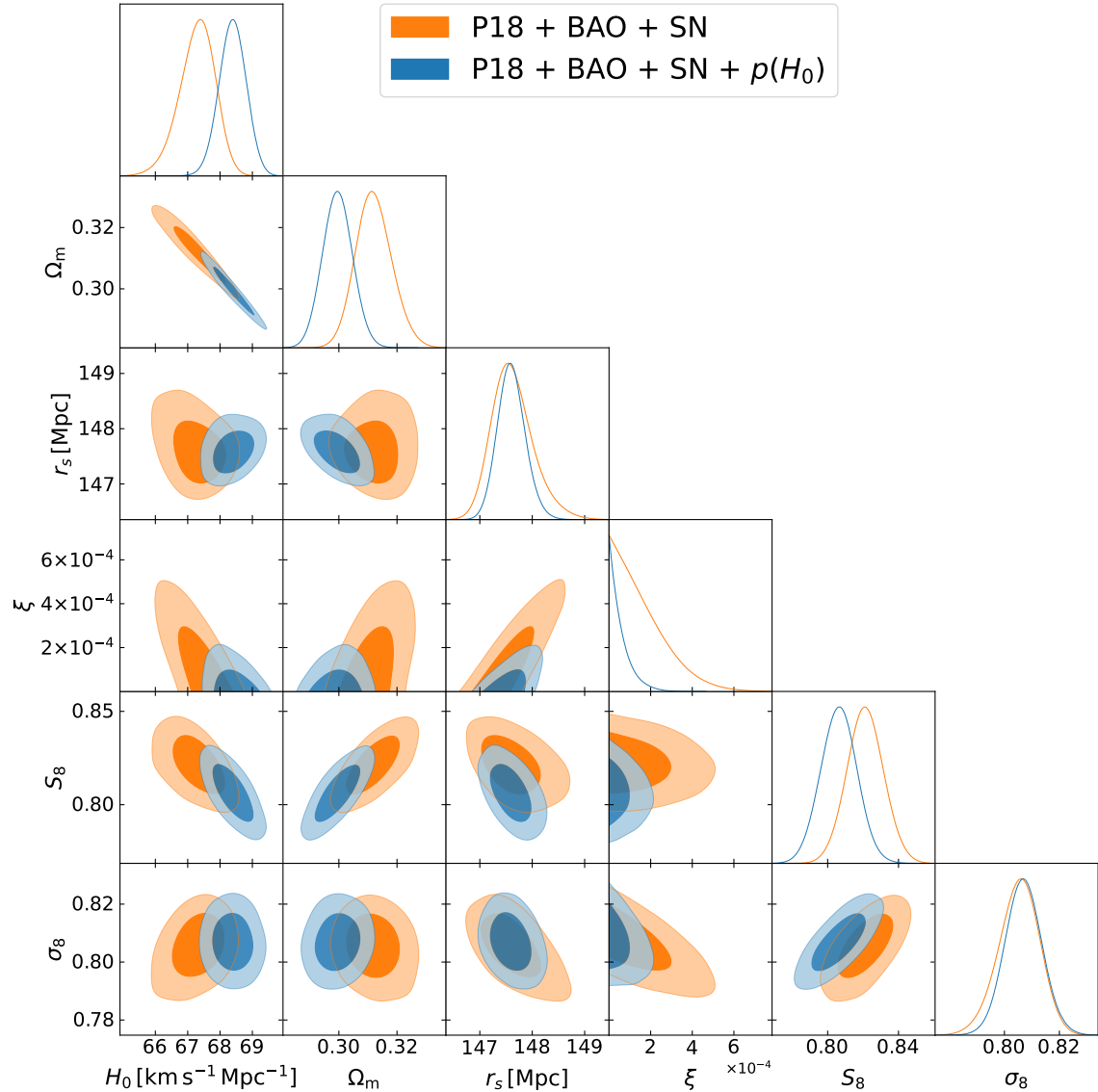


Figure 4. Marginalized joint 68% and 95% CL regions 2D parameter space using the combination CMB+BAO+SN (orange) and CMB+BAO+SN+ $p(H_0)$ (blue) for IG ($F = \xi\sigma^2$, $V = \lambda F^2/4$) in the phantom branch ($Z = -1$).

and consequently

$$\delta_m'' + \frac{3}{2a} \left(1 - \frac{4Z\xi}{3}\right) \delta_m' - \frac{3}{2a^2} \left(1 + \frac{16Z\xi}{3}\right) \delta_m \simeq 0. \quad (3.12)$$

In the weak coupling regime for $\xi \ll 1$, which turns out to be the range allowed from observations, the leading-order growing solution of Eq. (3.12) goes as $\delta_m \sim a^{1+4Z\xi}$ showing a slower (faster) growth of structures compared to the Λ CDM case for $Z < 0$ ($Z > 0$) during the matter dominated era.

We show the results for most of the combination of datasets on Fig. 6 (in Appendix E, we show a comparison between P18+BAO and P18+BAO+FS). The marginal-

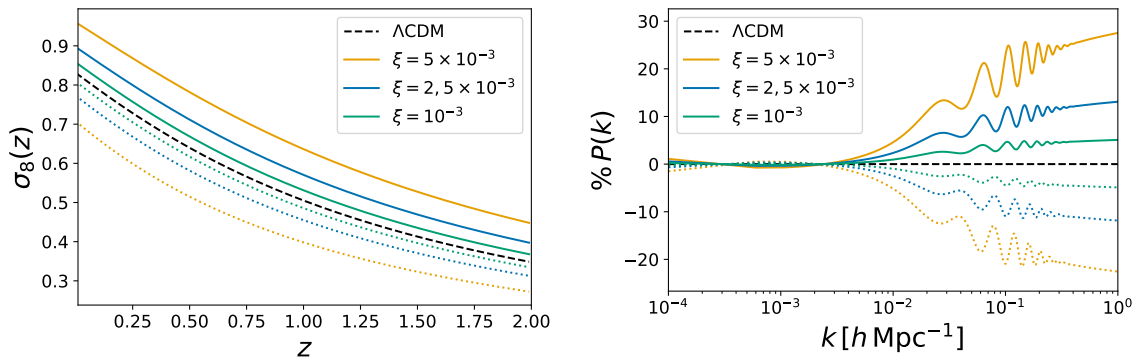


Figure 5. Time evolution of the amplitude of matter perturbation within spheres of radius $8 h^{-1} \text{ Mpc}$ (left panel) and relative differences of the linear matter power spectrum at $z = 0$ with respect to Λ CDM (right panel) for different values of the coupling parameter ξ in the standard branch (solid lines) and in the phantom one (dashed lines) for IG ($F = \xi\sigma^2$, $V = \lambda F^2/4$).

ized upper bound on the coupling parameter ξ at 95% CL corresponds to < 0.0024 for FS+SN, < 0.0018 for P18, < 0.00046 for P18+BAO, and < 0.00040 for P18+BAO+SN; see Tab. 1 for the constraints on all the parameters.

In Fig. 6, we see the larger marginalized uncertainties for the analysis without CMB information, i.e. combining FS with SN and a Gaussian prior on ω_b motivated from BBN, and the analysis with CMB alone. In these cases larger value of ξ can be accommodated by changes in the density parameters and in the scalar spectral index.

The marginalized means and uncertainties for the Hubble constant H_0 [$\text{km s}^{-1} \text{ Mpc}^{-1}$] at 68% CL correspond to 67.4 ± 1.8 for FS+SN, $63.6_{-1.9}^{+2.7}$ for P18, $67.17_{-0.50}^{+0.64}$ for P18+BAO, and $67.29_{-0.47}^{+0.60}$ for P18+BAO+SN; all of them are lower than the corresponding results we found in the standard branch, see Refs. [19, 79]. The upper bound on ξ becomes much tighter, i.e. $\xi < 0.00016$ at 95% CL, once we add a prior on H_0 in order to reproduce a larger value of the Hubble parameter, i.e. 68.34 ± 0.41 at 68% CL, see Fig. 4 and Tab. 4.

The marginalized constraint on the present value of σ_8 at 68% CL corresponds to 0.717 ± 0.049 for FS+SN, $0.784_{-0.015}^{+0.021}$ for P18, $0.799_{-0.009}^{+0.010}$ for P18+FS, and 0.8059 ± 0.0058 for P18+FS+SN. However, the combination $S_8 \equiv \sigma_8 \sqrt{\Omega_m/0.3}$, commonly used to quantify the tension between *Planck* and weak lensing of galaxies measurements, moves to the wrong direction. In order not to spoil the fit to CMB and galaxy measurements, an increase of the matter energy density is needed to compensate for the shifted position of the CMB acoustic peaks and of the BAO. Indeed, we find for S_8 0.744 ± 0.050 for FS+SN, $0.850_{-0.019}^{+0.016}$ for P18, $0.831_{-0.012}^{+0.011}$ for P18+FS, and 0.825 ± 0.012 for P18+FS+SN at 68% CL, resulting to be larger than in the standard branch as shown in Fig. 3.

The constraints found are at odds with the parameter space free from ghost which corresponds for IG to $\xi > 1/6$ according to Eqs. (2.8)-(2.9). Note that, this condition for ξ can be relaxed if one considers a more general Lagrangian with respect to the

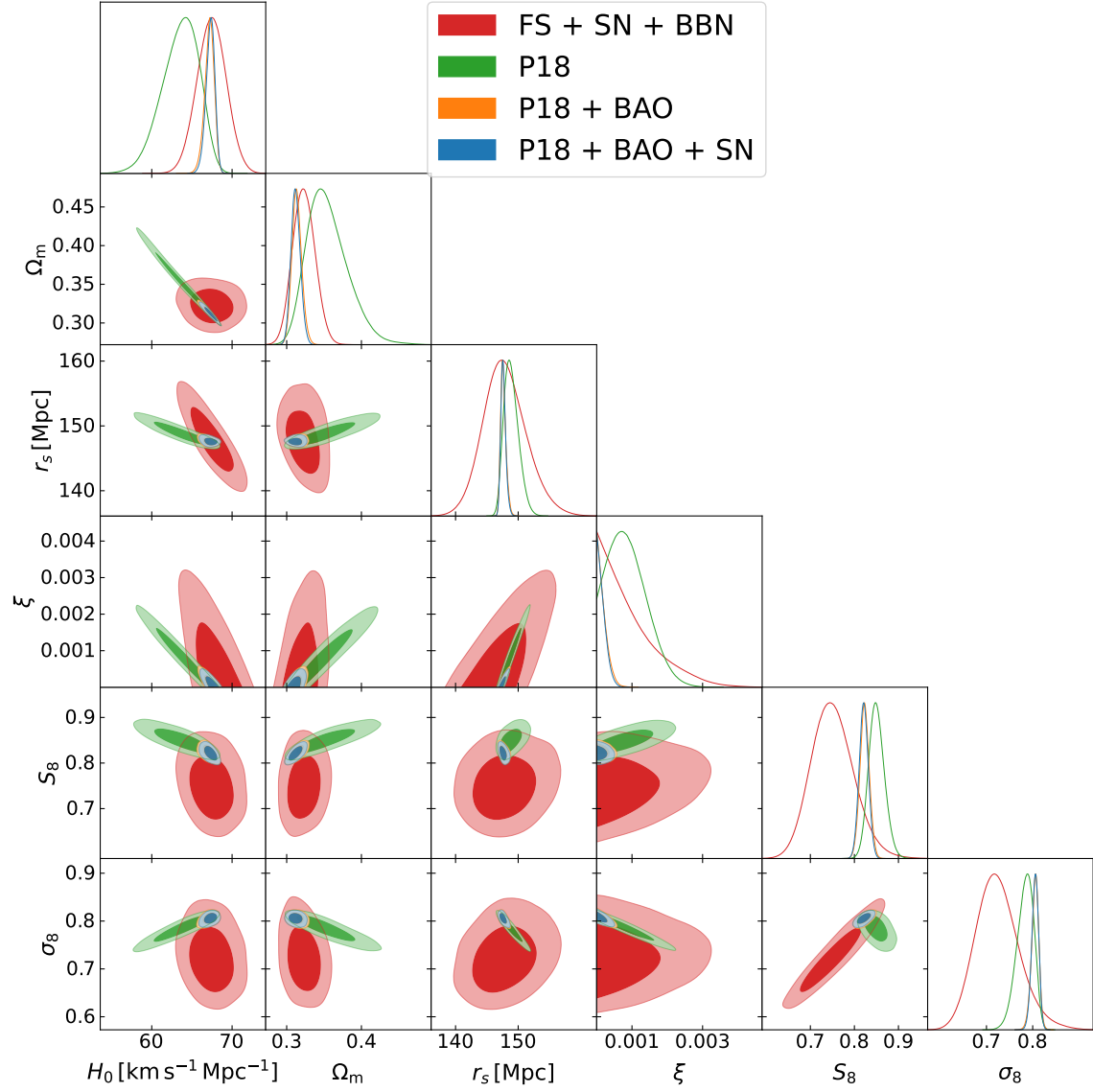


Figure 6. Marginalized joint 68% and 95% CL regions 2D parameter space using the CMB-independent combination FS+SN (red), P18 (green), the combination P18+BAO (orange), and the combination P18+BAO+SN (blue) for IG ($F = \xi\sigma^2$, $V = \lambda F^2/4$) in the phantom branch ($Z = -1$).

one introduced in Eq. (2.1). Higher order terms in the kinetic energy $X \equiv -\partial_\mu\sigma\partial^\mu\sigma/2$ [80] appear in low-energy effective string theory [81] or in tachyon condensation [82]. In a more general Lagrangian containing also a Galileon term G_3 [83, 84] as in $\mathcal{L} = G_4(\sigma)R + G_2(\sigma, X) + G_3(\sigma, X)\square\sigma$, the conditions for the avoidance of such instabilities are

$$q_s \equiv 4G_4\{G_{2X} + 2G_{3\sigma} + \dot{\sigma}[(G_{2XX} + G_{3X\sigma})\dot{\sigma} - 6G_{3XH}]\} + 3(2G_{4\sigma} + G_{3X}\dot{\sigma}^2)^2 > 0 \quad (3.13)$$

$$c_s^2 \equiv [4G_{2X}G_4 + 8G_{3\sigma}G_4 + (6G_{4\sigma}^2 - G_{3X}\dot{\sigma}^2)(2G_{4\sigma}^2 + G_{3X}\dot{\sigma}^2) - 8G_4(G_{3X}\ddot{\sigma} + 2G_{3X}H\dot{\sigma} + G_{3X\sigma}\dot{\sigma}^2)]/q_s > 0, \quad (3.14)$$

which reduce to Eqs. (2.8)-(2.9) when $G_3 = 0$; but, in general, depending on the functional form of the cubic interaction term and its magnitude, can allow for $\xi < 1/6$ while maintaining the theory free of ghost and Laplacian instabilities [77, 85–87].

3.2 Phantom non-minimal coupling

For NMC+ (NMC-) [14], with coupling $F(\sigma) = N_{\text{Pl}}^2 + \xi\sigma^2$ and coupling $V(\sigma) = \lambda F^2(\sigma)/4$, we sample on the dimensionless parameter $\Delta\tilde{N}_{\text{Pl}} \equiv N_{\text{Pl}}/M_{\text{Pl}} - 1$ and ξ .

We show the results for all the combinations of datasets on Fig. 7 for NMC+ and for NMC- in Fig. 8. Marginalized constraints on cosmological parameters are consistent to the results obtained for IG for each combination of datasets. The marginalized limits on the coupling parameters for NMC+ (NMC-) at 95% CL correspond to $\xi < 0.0015$ (> -0.039) and $N_{\text{Pl}} > 0.91$ (< 1.18) for P18+BAO, and to $\xi < 0.0019$ (> -0.027) and $N_{\text{Pl}} > 0.83$ (< 1.21) for P18+BAO+SN; see Tabs. 2 and 3 for the constraints on all the parameters. As observed in Refs. [14, 19], there is a strong degeneracy between the coupling parameters N_{Pl} and ξ for the form of non-minimal coupling $F(\sigma) = N_{\text{Pl}}^2 + \xi\sigma^2$. Since cosmological observables are affected by contributions $\mathcal{O}(\xi\sigma^2/N_{\text{Pl}}^2)$, it is possible to compensate the effects due to a large value of $|\xi|$ increasing $|\tilde{N}_{\text{Pl}} - 1|$ and vice versa.

In this case Eqs. (2.8)-(2.9) reduce to

$$\left(\frac{N_{\text{Pl}}}{\xi\sigma}\right)^2 + \frac{1}{\xi} < 6. \quad (3.15)$$

Also in this case, a large portion of the allowed parameter space is at odds with Eq. (3.15) despite the larger number of degrees of freedom.

3.3 Phantom early modified gravity

For EMG [20], with coupling $F(\sigma) = M_{\text{Pl}}^2 + \xi\sigma^2$ and potential $V(\sigma) = \Lambda + \lambda\sigma^4/4$, we sample on the quantity ξ and V_0 where $\lambda \equiv -10^{2V_0}/M_{\text{Pl}}^4$. In this case the scalar field decays into the minimum of the potential, i.e. $\sigma = 0$, and we do not have to impose the boundary condition (3.1) being automatically satisfied for each initial value of scalar field. This leads to a third free parameter which we identify with the initial value of the scalar field $\sigma_{\text{ini}} [M_{\text{Pl}}]$.

In Fig. 9, we compare the background evolution and spectra of EMG in the standard branch ($Z = 1$) to the phantom branch case ($Z = -1$). The evolution of the scalar field σ is very similar in the two cases. Starting with the scalar field at rest in the radiation era, it starts to grow around the recombination driven by the coupling to the non-relativistic matter component and it is subsequently driven into damped coherent oscillations around the minimum of the quartic potential. The different evolution of the coupling function, which increase in the branch with standard kinetic term while decreasing in the phantom branch before the scalar field starts to decay, due to the different sign of the coupling parameter ξ induces different effects on the spectra.

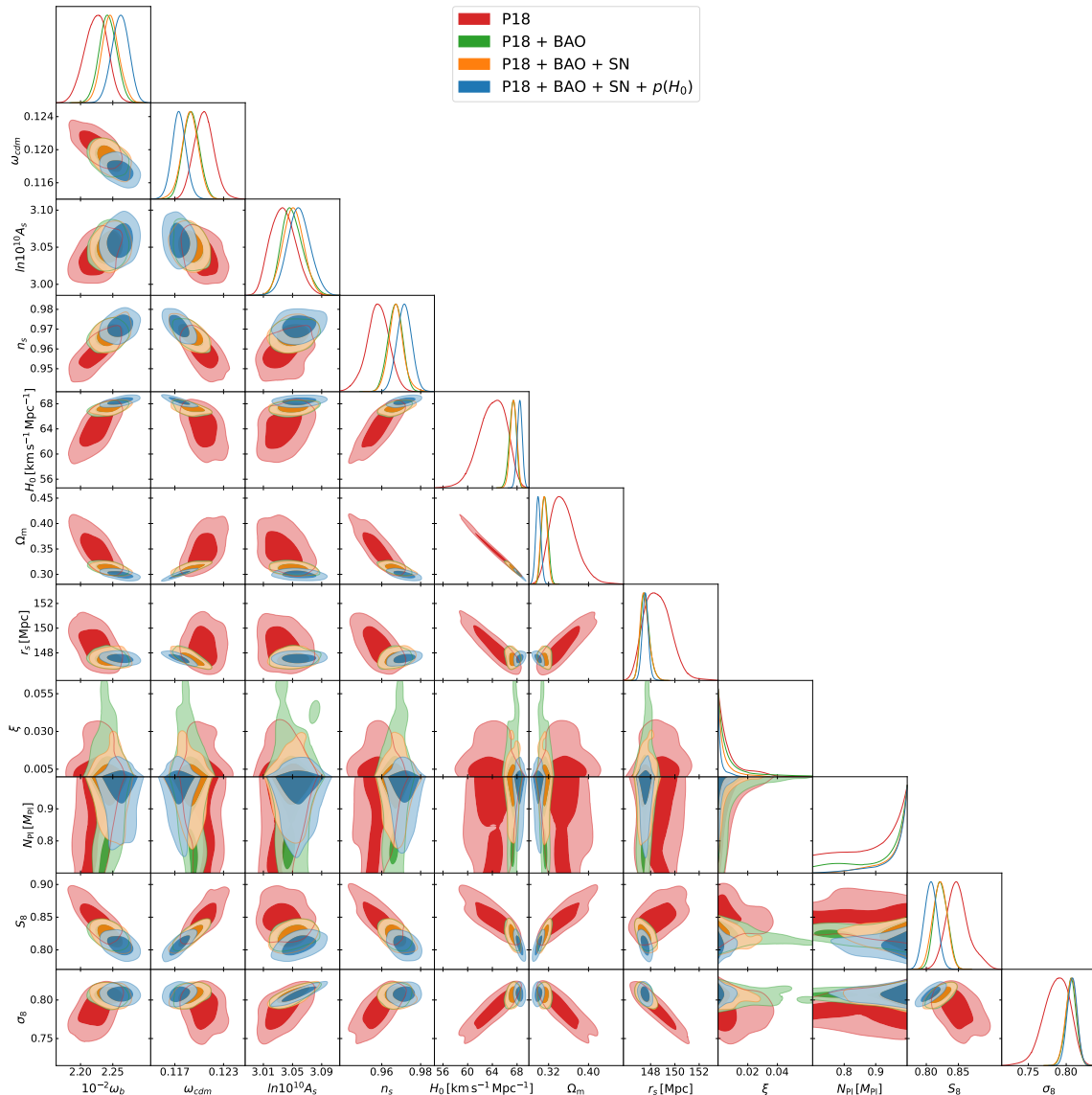


Figure 7. Marginalized joint 68% and 95% CL regions 2D parameter space using using the P18 (green), the combination P18+BAO (orange), and the combination P18+BAO+SN (blue) for NMC+ ($F = N_{\text{Pl}}^2 + \xi\sigma^2$, $V = \lambda F^2/4$) in the phantom branch ($Z = -1$).

The acoustic peaks of the CMB temperature anisotropies angular power spectrum are shifted to right in the standard branch ($Z = 1$) when the scalar field starts to move before recombination ($V_0 = 2$) and in the phantom branch ($Z = -1$) if the scalar field decays after recombination ($V_0 = -1$), vice versa they shift to the left with respect the Λ CDM case. The situation is different on the linear matter power spectrum were we observe a suppression of power in the standard branch ($Z = 1$) despite the value of V_0 and an increase of power at small scales in the phantom branch ($Z = -1$). This highlights the importance of the combination of combining early- and late-time probes in order to break the degeneracy between the extra parameters of the model and also

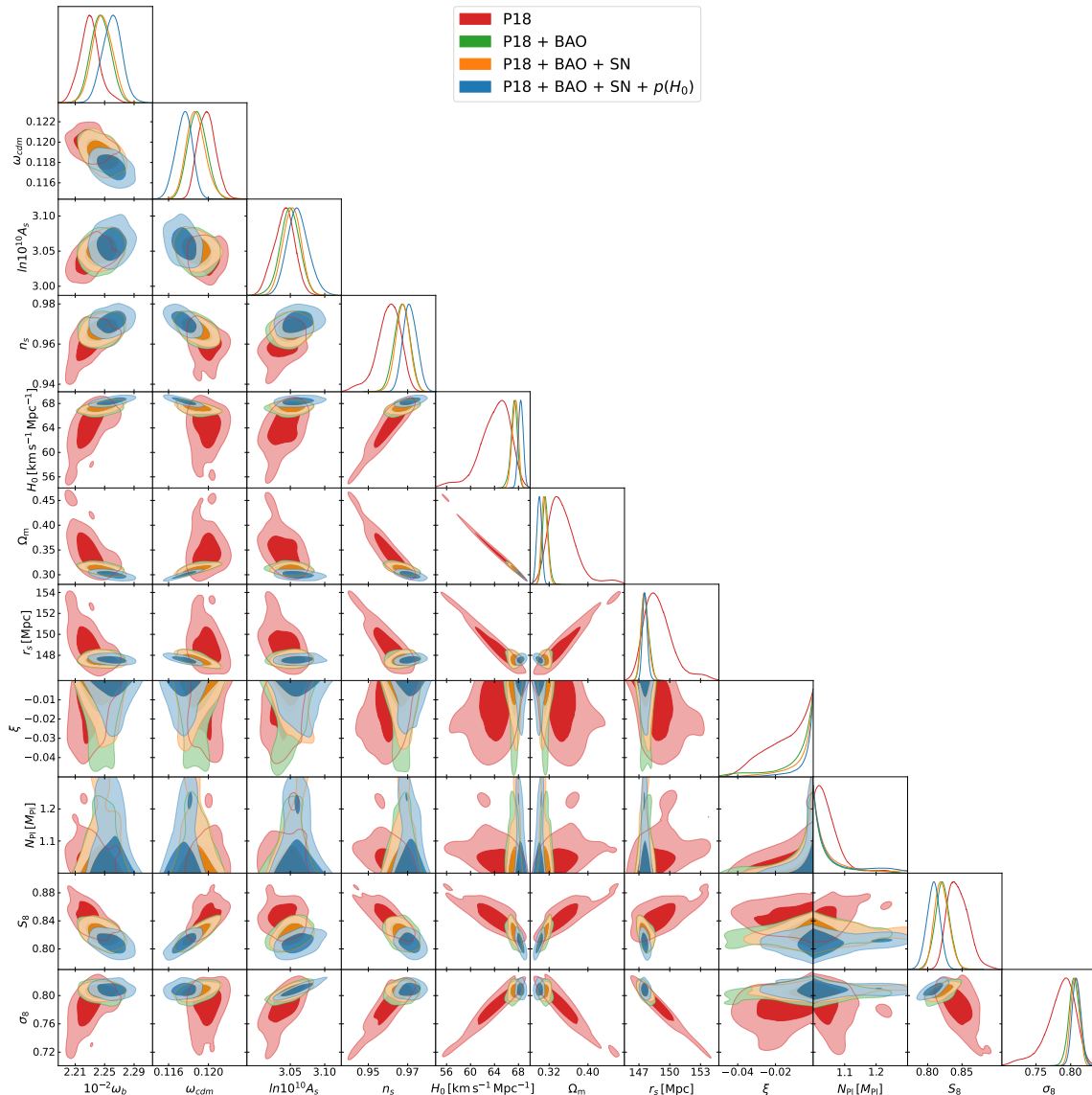


Figure 8. Marginalized joint 68% and 95% CL regions 2D parameter space using using the P18 (red), the combination P18+BAO (green), the combination P18+BAO+SN (orange), and the combination P18+BAO+SN+ $p(H_0)$ (blue) for NMC- ($F = N_{\text{p1}}^2 + \xi\sigma^2$, $V = \lambda F^2/4$) in the phantom branch ($Z = -1$).

to discriminate between the two different branches.

We show the results for the combinations of datasets P18+BAO+SN and P18+BAO+SN+ $p(H_0)$ on Fig. 10. In this case we find that ξ is not constrained by data on the prior considered $[-0.1, 0]$. For this reason, we show constraints on the combination $\xi\sigma_{\text{ini}}^2 [M_{\text{p1}}^2]$ (connected to the additional contribution to the expansion rate evolution (3.2) before recombination). The marginalized upper bound on the coupling combination $\xi\sigma_{\text{ini}}^2$ at 95% CL corresponds to > -0.0026 for P18+BAO+SN and when we include the Gaussian prior on the Hubble parameter we obtain at 95%

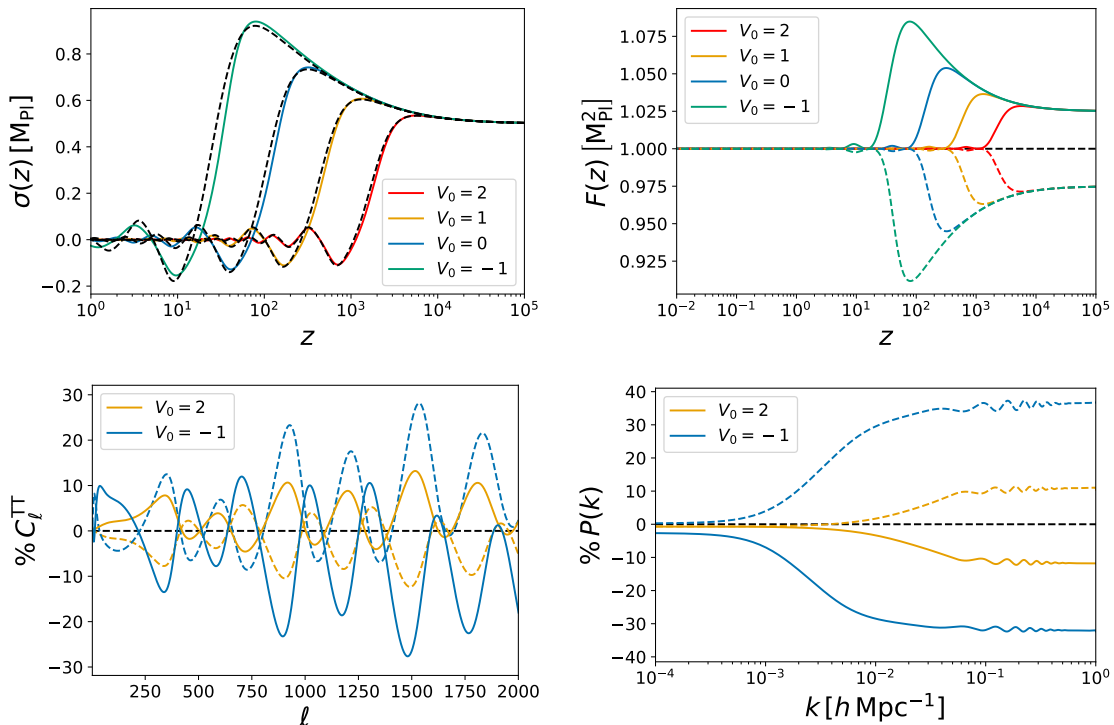


Figure 9. Time evolution of the scalar field σ (upper left panel) and of the coupling to the Ricci scalar $F(\sigma)$ (upper right panel). Relative differences of the CMB temperature anisotropies power spectrum with respect to the Λ CDM case (bottom left panel) and of the linear matter power spectrum at $z = 0$ (bottom right panel). Different lines correspond to different value of the amplitude of the effective potential V_0 for $|\xi| = 0.1$ in the standard branch (solid lines) and in the phantom one (dashed lines) for EMG ($F = M_{\text{Pl}}^2 + \xi\sigma^2$, $V = \Lambda + \lambda\sigma^4/4$).

CL -0.006 ± 0.005 . Analogously, for the initial value of the scalar field $\sigma_{\text{ini}} [M_{\text{Pl}}]$ we find < 0.45 for P18+BAO+SN and $0.35_{-0.15}^{+0.17}$ for P18+BAO+SN+ $p(H_0)$ both at 95% CL. Also V_0 is not well constrained. We find a 95% CL upper bound only when we include the Gaussian prior on the Hubble parameter corresponding to $V_0 < 0.81$.

The marginalized means and uncertainties for the Hubble constant H_0 [$\text{km s}^{-1} \text{ Mpc}^{-1}$] at 68% CL correspond to $68.44_{-0.79}^{+0.62}$ for P18+BAO+SN and $70.18_{-0.68}^{+0.59}$ for P18+BAO+SN+ $p(H_0)$. The marginalized constraints on S_8 correspond to $S_8 = 0.827 \pm 0.011$ for P18+BAO+SN and $S_8 = 0.822 \pm 0.010$ for P18+BAO+SN+ $p(H_0)$. See Tab. 5 for the constraints on all the parameters.

4 Conclusions

We have studied the dynamics and inferred the cosmological constraints for modified gravity models with a nonminimally coupled scalar with a kinetic term which can also have a negative sign. For stable models with an effectively massless scalar field σ , like IG and NMC, the change of sign in front of the kinetic term of the scalar field modifies

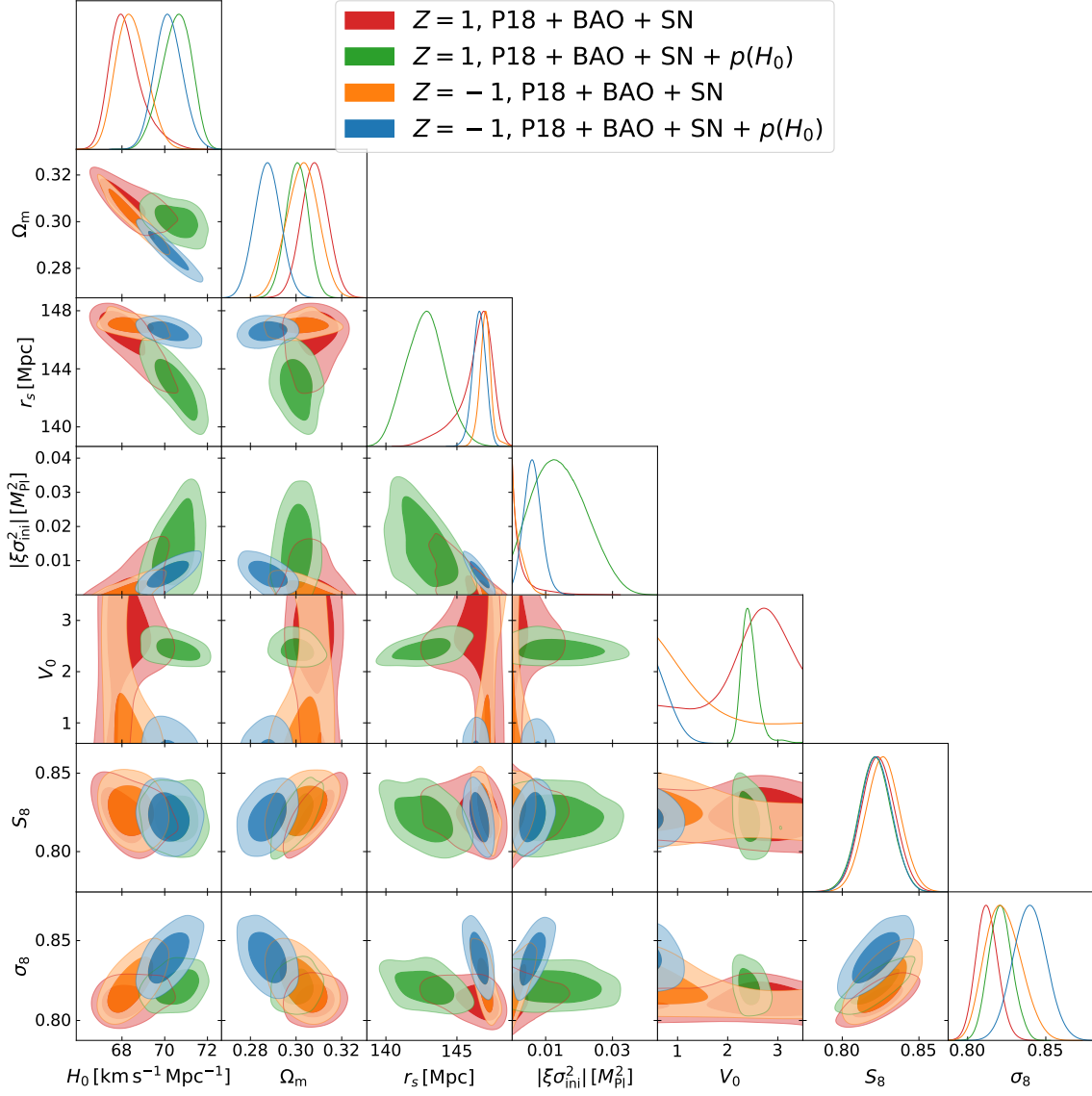


Figure 10. Marginalized joint 68% and 95% CL regions 2D parameter space using P18+BAO+SN (orange) and the combination P18+BAO+SN+ $\rho(H_0)$ (blue) for EMG ($F = M_{\text{Pl}}^2 + \xi\sigma^2$, $V = \Lambda + \lambda\sigma^4/4$) in the phantom branch ($Z = -1$).

the evolution of the scalar field which is at rest during the radiation-dominated epoch and evolves like $\sigma \sim a^{2Z\xi}$ during the matter-dominated era.

We have shown the effect of the sign of the kinetic term on cosmological observables. We have computed the marginalized constraints for different combination of cosmological datasets by allowing the coupling to the Ricci scalar and the rest of cosmology (standard cosmological parameters and nuisance ones) to vary. Combining *Planck* 2018 DR3 measurements with BAO from BOSS and eBOSS, and uncalibrated SN Ia from the Pantheon sample we constrain the coupling parameters at 95% CL to $\xi < 0.00040$ for $F(\sigma) = \xi\sigma^2$ and for $F(\sigma) = N_{\text{Pl}}^2 + \xi\sigma^2$ to $\xi < 0.0019$ (> -0.027) and

$N_{\text{PI}} > 0.83$ (< 1.21).

Nonminimally coupled scalar-tensor theories with early-time deviation from GR predictions usually lead to higher values of the Hubble parameter H_0 , a lower value of the matter density parameter Ω_m , and a larger value of the σ_8 [19, 77, 78]. In their phantom construction, the modified evolution of the scalar field, connected to a different time evolution of the effective gravitational constant, inverts the degeneracy between these parameters and the coupling ones. Indeed, we find a lower values of both σ_8 and H_0 compared to the branch with standard kinetic term.

We have also studied the phantom version of the EMG model introduced in Ref. [20]. While the evolution of the scalar field is very similar, with the quartic potential leading the scalar field to decay into damped coherent oscillations, different signatures appear on the cosmological observables. Compared to the Λ CDM model, the CMB acoustic peaks of the CMB are shifted to right in the standard branch ($Z = 1$) when the scalar field starts to move before recombination ($V_0 = 2$) and in the phantom branch ($Z = -1$) if the scalar field decays after recombination ($V_0 = -1$), vice versa they shift to the left. Matter perturbations on sub-horizon scales are suppressed in the standard branch ($Z = 1$) and enhanced in the phantom branch ($Z = -1$) despite the value of amplitude of the self-interaction term parameterized by V_0 .

The allowed parameter space for the coupling parameters by our analysis is at odds with the parameter space free from ghosts and Laplacian instabilities. It would be interesting to understand if instead there are healthy scalar-tensor theories which retain the possibility to alleviate the current tensions between different cosmological observations.

Acknowledgments

MB and FF acknowledge financial support from the INFN InDark initiative and from the COSMOS network (www.cosmosnet.it) through the ASI (Italian Space Agency) Grants 2016-24-H.0 and 2016-24-H.1-2018, as well as 2020-9-HH.0 (participation in LiteBIRD phase A). This work has made use of computational resources of INAF OAS Bologna and of the CNAF HPC cluster in Bologna.

A Tables

	P18	P18 + BAO	P18 + BAO + SN
ω_b	0.02223 ± 0.00017	0.02244 ± 0.00013	0.02245 ± 0.00013
ω_c	0.1204 ± 0.0012	0.11896 ± 0.00099	0.11882 ± 0.00096
H_0 [km s ⁻¹ Mpc ⁻¹]	$63.6^{+2.7}_{-1.9}$	$67.17^{+0.65}_{-0.48}$	$67.29^{+0.60}_{-0.47}$
τ	0.0523 ± 0.0071	$0.0584^{+0.0070}_{-0.0083}$	$0.0584^{+0.0068}_{-0.0076}$
$\ln(10^{10}A_s)$	3.037 ± 0.015	$3.051^{+0.014}_{-0.016}$	3.051 ± 0.014
n_s	$0.9574^{+0.0067}_{-0.0057}$	0.9668 ± 0.0038	0.9671 ± 0.0036
ξ	< 0.0018 (95% CL)	< 0.00046 (95% CL)	< 0.00040 (95% CL)
γ_{PN}	> 0.9928 (95% CL)	> 0.9982 (95% CL)	> 0.9984 (95% CL)
$\delta G_{\text{N}}/G_{\text{N}}(z=0)$	< 0.057 (95% CL)	< 0.014 (95% CL)	< 0.012 (95% CL)
$10^{13}\dot{G}_{\text{N}}/G_{\text{N}}(z=0)$ [yr ⁻¹]	< 2.43 (95% CL)	< 0.57 (95% CL)	< 0.50 (95% CL)
$G_{\text{N}}/G(z=0)$	$0.9982^{+0.0013}_{-0.00074}$	$0.99965^{+0.00033}_{-0.00013}$	$0.99968^{+0.00030}_{-0.00012}$
Ω_m	$0.354^{+0.020}_{-0.032}$	$0.3135^{+0.0059}_{-0.0068}$	$0.3120^{+0.0056}_{-0.0065}$
σ_8	$0.784^{+0.021}_{-0.015}$	$0.8053^{+0.0083}_{-0.0069}$	$0.8053^{+0.0078}_{-0.0066}$
S_8	$0.850^{+0.016}_{-0.019}$	0.823 ± 0.011	0.821 ± 0.010
r_s [Mpc]	$148.89^{+0.8}_{-1.4}$	$147.62^{+0.31}_{-0.50}$	$147.62^{+0.29}_{-0.44}$
$\Delta\chi^2$	-2.8	0	-0.5

Table 1. Constraints on the main and derived parameters (at 68% CL if not otherwise stated) considering P18 in combination with BAO and BAO+SN for the **IG** model.

	P18	P18 + BAO	P18 + BAO + SN
ω_b	$0.02224^{+0.00018}_{-0.00016}$	0.02246 ± 0.00013	$0.02246^{+0.00011}_{-0.00014}$
ω_c	0.1206 ± 0.0012	$0.1190^{+0.0014}_{-0.0011}$	0.1189 ± 0.0010
H_0 [km s ⁻¹ Mpc ⁻¹]	$64.1^{+2.6}_{-1.7}$	67.28 ± 0.59	67.42 ± 0.52
τ	0.0514 ± 0.0081	0.0590 ± 0.0052	0.0583 ± 0.0071
$\ln(10^{10} A_s)$	$3.037^{+0.015}_{-0.023}$	$3.0517^{+0.0074}_{-0.015}$	3.051 ± 0.014
n_s	$0.9580^{+0.0058}_{-0.0047}$	0.9673 ± 0.0042	0.9674 ± 0.0039
ξ	< 0.030 (95% CL)	< 0.015 (95% CL)	< 0.019 (95% CL)
$N_{\text{PI}} [M_{\text{Pl}}]$	–	> 0.91 (95% CL)	> 0.83 (95% CL)
γ_{PN}	> 0.9941 (95% CL)	> 0.9986 (95% CL)	> 0.9987 (95% CL)
β_{PN}	> 0.999965 (95% CL)	> 0.999994 (95% CL)	> 0.999994 (95% CL)
$\delta G_{\text{N}}/G_{\text{N}} (z=0)$	< 0.052 (95% CL)	< 0.011 (95% CL)	< 0.012 (95% CL)
$10^{13} \dot{G}_{\text{N}}/G_{\text{N}} (z=0)$ [yr ⁻¹]	< 1.94 (95% CL)	< 0.42 (95% CL)	< 0.40 (95% CL)
$G_{\text{N}}/G (z=0)$	$1.00134^{+0.00063}_{-0.0011}$	$1.000255^{+0.000097}_{-0.00024}$	$1.000221^{+0.000084}_{-0.00023}$
Ω_m	$0.349^{+0.017}_{-0.030}$	$0.3121^{+0.0068}_{-0.0056}$	0.3110 ± 0.0061
σ_8	$0.788^{+0.021}_{-0.013}$	0.8069 ± 0.0069	$0.8064^{+0.0079}_{-0.0065}$
S_8	$0.849^{+0.013}_{-0.019}$	$0.823^{+0.014}_{-0.009}$	$0.821^{+0.012}_{-0.011}$
r_s [Mpc]	$148.56^{+0.90}_{-1.3}$	$147.54^{+0.30}_{-0.48}$	$147.52^{+0.27}_{-0.44}$
$\Delta\chi^2$	-1.5	0	-0.5

Table 2. Constraints on the main and derived parameters (at 68% CL if not otherwise stated) considering P18 in combination with BAO and BAO+SN for the **NMC+** model.

	P18	P18 + BAO	P18 + BAO + SN
ω_b	0.02230 ± 0.00014	0.02245 ± 0.00013	0.02247 ± 0.00013
ω_c	$0.11982^{+0.00068}_{-0.0011}$	0.11891 ± 0.00094	$0.11875^{+0.00078}_{-0.0010}$
H_0 [km s ⁻¹ Mpc ⁻¹]	$64.1^{+3.1}_{-2.1}$	$67.26^{+0.59}_{-0.45}$	$67.44^{+0.57}_{-0.45}$
τ	$0.0548^{+0.0072}_{-0.0059}$	$0.0573^{+0.0061}_{-0.0074}$	0.0590 ± 0.0068
$\ln(10^{10} A_s)$	$3.041^{+0.017}_{-0.013}$	3.049 ± 0.014	$3.052^{+0.014}_{-0.012}$
n_s	$0.9604^{+0.0067}_{-0.0045}$	$0.9669^{+0.0043}_{-0.0035}$	0.9675 ± 0.0036
ξ	> -0.036 (95% CL)	> -0.039 (95% CL)	> -0.027 (95% CL)
$N_{\text{PI}} [M_{\text{Pl}}]$	< 1.13 (95% CL)	< 1.18 (95% CL)	< 1.21 (95% CL)
γ_{PN}	> 0.988 (95% CL)	> 0.998 (95% CL)	> 0.998 (95% CL)
β_{PN}	< 1.00018 (95% CL)	< 1.000022 (95% CL)	< 1.000017 (95% CL)
$\delta G_{\text{N}}/G_{\text{N}} (z=0)$	< 0.060 (95% CL)	< 0.012 (95% CL)	< 0.010 (95% CL)
$10^{13} \dot{G}_{\text{N}}/G_{\text{N}} (z=0)$ [yr ⁻¹]	< 3.85 (95% CL)	< 0.62 (95% CL)	< 0.50 (95% CL)
$G_{\text{N}}/G (z=0)$	$1.00224^{+0.00080}_{-0.0021}$	$1.00037^{+0.00012}_{-0.00037}$	$1.00030^{+0.00012}_{-0.00030}$
Ω_m	$0.348^{+0.021}_{-0.033}$	$0.3125^{+0.0052}_{-0.0065}$	$0.3106^{+0.0050}_{-0.0068}$
σ_8	$0.786^{+0.025}_{-0.011}$	0.8047 ± 0.0076	0.8064 ± 0.0062
S_8	$0.844^{+0.011}_{-0.018}$	0.821 ± 0.011	$0.8204^{+0.0091}_{-0.012}$
r_s [Mpc]	$148.91^{+0.77}_{-1.6}$	$147.60^{+0.28}_{-0.43}$	$147.57^{+0.30}_{-0.40}$
$\Delta\chi^2$	-2.8	0	-0.3

Table 3. Constraints on the main and derived parameters (at 68% CL if not otherwise stated) considering P18 in combination with BAO and BAO+SN for the **NMC-** model.

	IG	NMC+	NMC-
ω_b	$0.02260^{+0.00012}_{-0.00014}$	0.02262 ± 0.00013	$0.02260^{+0.00014}_{-0.00012}$
ω_c	0.11747 ± 0.00086	0.11752 ± 0.00086	$0.11753^{+0.00095}_{-0.00069}$
H_0 [km s ⁻¹ Mpc ⁻¹]	68.34 ± 0.41	$68.42^{+0.44}_{-0.36}$	68.38 ± 0.41
τ	$0.0617^{+0.0067}_{-0.0085}$	$0.0636^{+0.0071}_{-0.0081}$	$0.0644^{+0.0068}_{-0.0090}$
$\ln(10^{10} A_s)$	$3.055^{+0.013}_{-0.017}$	$3.059^{+0.014}_{-0.016}$	$3.061^{+0.014}_{-0.017}$
n_s	0.9711 ± 0.0036	0.9716 ± 0.0037	0.9712 ± 0.0035
ξ	< 0.000075 (95% CL)	< 0.0096 (95% CL)	> -0.022 (95% CL)
$N_{\text{PI}} [M_{\text{PI}}]$	0	> 0.82 (95% CL)	< 1.24 (95% CL)
γ_{PN}	> 0.9993 (95% CL)	> 0.9995 (95% CL)	> 0.9994 (95% CL)
β_{PN}	1	> 0.999999 (95% CL)	< 1.000004 (95% CL)
$\delta G_{\text{N}}/G_{\text{N}} (z=0)$	< 0.0056 (95% CL)	< 0.0041 (95% CL)	< 0.0042 (95% CL)
$10^{13} \dot{G}_{\text{N}}/G_{\text{N}} (z=0)$ [yr ⁻¹]	< 0.23 (95% CL)	< 0.16 (95% CL)	< 0.19 (95% CL)
$G_{\text{N}}/G (z=0)$	$0.99987^{+0.00013}_{-0.000042}$	$1.000080^{+0.000028}_{-0.000090}$	$1.000102^{+0.000043}_{-0.00011}$
Ω_{m}	0.2999 ± 0.0050	$0.2994^{+0.0046}_{-0.0052}$	$0.2997^{+0.0053}_{-0.0047}$
σ_8	$0.8055^{+0.0059}_{-0.0069}$	0.8078 ± 0.0066	0.8086 ± 0.0063
S_8	0.805 ± 0.010	0.807 ± 0.010	0.8082 ± 0.0094
r_s [Mpc]	$147.63^{+0.23}_{-0.29}$	147.56 ± 0.25	$147.58^{+0.21}_{-0.24}$

Table 4. Constraints on the main and derived parameters (at 68% CL if not otherwise stated) considering the combination with P18+BAO+SN+ $p(H_0)$ for **IG**, **NMC+**, and **NMC-**.

	P18 + BAO + SN	P18 + BAO + SN + $p(H_0)$
ω_b	0.02246 ± 0.00014	0.02255 ± 0.00014
ω_c	0.1194 ± 0.0010	0.11900 ± 0.00099
H_0 [km s ⁻¹ Mpc ⁻¹]	$68.44^{+0.62}_{-0.79}$	$70.18^{+0.59}_{-0.68}$
τ	0.0536 ± 0.0080	$0.0503^{+0.0085}_{-0.0073}$
$\ln(10^{10} A_s)$	3.043 ± 0.016	$3.035^{+0.017}_{-0.015}$
n_s	$0.9671^{+0.0036}_{-0.0042}$	0.9687 ± 0.0038
$\xi \sigma_{\text{ini}}^2 [M_{\text{PI}}^2]$	> -0.0057 (95% CL)	$-0.0062^{+0.0028}_{-0.0023}$
V_0	–	< 0.81 (95% CL)
$\sigma_{\text{ini}} [M_{\text{PI}}]$	< 0.446 (95% CL)	$0.348^{+0.062}_{-0.097}$
Ω_{m}	0.3028 ± 0.0068	0.2875 ± 0.0056
σ_8	$0.823^{+0.010}_{-0.013}$	0.840 ± 0.011
S_8	0.827 ± 0.011	0.822 ± 0.010
r_s [Mpc]	147.00 ± 0.40	146.56 ± 0.46

Table 5. Constraints on the main and derived parameters (at 68% CL if not otherwise stated) considering P18 in combination with BAO+SN and BAO+SN+ $p(H_0)$ for the **EMG** model.

B Background equations

Starting from Eq. 2.1, it is possible to write down the equations governing the background evolution. Specializing to a spatially flat Friedmann-Lemaître-Robertson-Walker

P18+BAO+SN	IG	NMC+	NMC-	EMG ($Z = 1$)	EMG ($Z = -1$)
<i>Planck</i> high- ℓ TTTEEE	-1.2	-1.3	-1.6	-0.8	-0.6
<i>Planck</i> low- ℓ EE	0.4	0.4	1	0.1	-0.3
<i>Planck</i> low- ℓ TT	0.2	0.3	0.3	-0.2	0.5
<i>Planck</i> lensing	-0.2	-0.2	-0.3	0	0.8
BAO	0.2	0.2	0.2	0	-0.5
Pantheon	0.1	0.1	0.1	0	-0.2
Total	-0.5	-0.5	-0.3	-0.9	-0.3

P18+BAO+SN+ $p(H_0)$	IG	NMC+	NMC-	EMG ($Z = 1$)	EMG ($Z = -1$)
<i>Planck</i> high- ℓ TTTEEE	-1.2	-0.8	-1.4	-0.7	-6.5
<i>Planck</i> low- ℓ EE	0.8	0.4	0.7	0.4	-1.8
<i>Planck</i> low- ℓ TT	-0.1	-0.2	-0.2	-0.2	1.1
<i>Planck</i> lensing	-0.1	-0.1	-0.2	-0.1	0.6
BAO	0.1	0.1	0	0	5
Pantheon	0	0	0	0	0.4
H_0	0	0.2	0.6	-17.8	-13.7
Total	-0.5	-0.4	-0.5	-18.4	-14.9

Table 6. Best-fit $\Delta\chi^2$ with respect to the Λ CDM model for each dataset for the combination P18+BAO+SN (upper table) and P18+BAO+SN+ $p(H_0)$ (lower table) for **IG**, **NMC+**, **NMC-**, and **EMG**.

(FLRW) universe described by the line element

$$ds^2 = a^2(\eta) (-d\eta^2 + d\mathbf{x}^2) , \quad (\text{B.1})$$

where η is the conformal time and \mathbf{x} the spatial comoving coordinate. The Einstein equations are obtained by varying the action 2.1 with respect to the metric, they correspond to

$$G^\mu{}_\nu = \frac{1}{F} \left[T^\mu{}_\nu - \frac{Z}{2} \nabla^\mu \sigma \nabla_\nu \sigma - g^\mu{}_\nu V + (\nabla^\mu \nabla_\nu - g^\mu{}_\nu \square) F \right] \quad (\text{B.2})$$

where the energy-momentum tensor for a perfect fluid is given by

$$T_{\mu\nu} = pg_{\mu\nu} + (\rho + p)u_\mu u_\nu \quad (\text{B.3})$$

where a sum over all the species in the Universe is taken for granted, i.e. $\rho \equiv \sum_i \rho_i$ and $p \equiv \sum_i p_i$.

From Eq. (B.2), the Friedmann equations in Jordan frame are as follows

$$3F \mathcal{H}^2 = a^2 (\rho + V) + \frac{Z\sigma'^2}{2} - 3\mathcal{H}F' \quad (\text{B.4})$$

$$-2F \mathcal{H}' = \frac{a^2}{3} (\rho + 3p - 2V) + \frac{2}{3} Z\sigma'^2 + F'' \quad (\text{B.5})$$

and the Einstein trace (the Ricci scalar) equation results

$$a^2FR = a^2(\rho - 3p) + 4a^2V - 3F_\sigma(\sigma'' + 2\mathcal{H}\sigma') - (Z + 3F_{\sigma\sigma})\sigma'^2. \quad (\text{B.6})$$

Finally, the evolution equation of the scalar field σ is governed by the modified Klein-Gordon equation

$$\sigma'' + 2\mathcal{H}\sigma' - \frac{F_\sigma}{2ZF + 3F_\sigma^2} \left[a^2(\rho - 3p) + 4a^2 \left(V - \frac{F}{2F_\sigma} V_\sigma \right) - (Z + 3F_{\sigma\sigma})\sigma'^2 \right] = 0. \quad (\text{B.7})$$

C Linear perturbed equations

In the synchronous gauge, up to linear order in perturbed quantities, the perturbed FLRW metric is

$$ds^2 = a^2(\eta) \left[-d^2\eta + (\delta_{ij} + h_{ij})dx^i dx^j \right] \quad (\text{C.1})$$

where h_{ij} is the metric perturbation.

From this point on, we move in Fourier space for the calculation of the perturbed quantities. The scalar mode of h_{ij} can be express as a Fourier integral as

$$h_{ij}(\eta, \mathbf{x}) = \int d^3k e^{i\mathbf{k}\cdot\mathbf{x}} \left[\hat{k}_i \hat{k}_j h(\eta, \mathbf{k}) + \left(\hat{k}_i \hat{k}_j - \frac{\delta_{ij}}{3} \right) 6\xi(\eta, \mathbf{k}) \right] \quad (\text{C.2})$$

where $\hat{k}_i = k_i/k$ with $k = |\mathbf{k}|$ and $h \equiv \delta^{ij}h_{ij}$ is the Fourier transform of trace of $h_{ij}(\eta, \mathbf{x})$. We follow the conventions of Ref. [88].

C.1 The perturbed Einstein field equations

Splitting the Einstein tensor as the sum of the background (mean) part $\bar{G}_{\mu\nu}$ and its corresponding perturbation $\delta G_{\mu\nu}$, i.e. $G_{\mu\nu} = \bar{G}_{\mu\nu} + \delta G_{\mu\nu}$, the scalar perturbations in synchronous gauge are usually presented as time-time, longitudinal time-space, trace space-space, and longitudinal traceless space-space parts of the Einstein equations in Fourier space as follow

$$\begin{aligned} \xi k^2 - \frac{\mathcal{H}h'}{2} &= a^2 \frac{\delta G^0_0}{2} \\ &= 4\pi G a^2 \delta T^0_0, \end{aligned} \quad (\text{C.3})$$

$$\begin{aligned} k^2 \xi' &= a^2 \frac{\nabla^i \delta G^0_i}{2} \\ &= 4\pi G a^2 (\bar{\rho} + \bar{p})\theta, \end{aligned} \quad (\text{C.4})$$

$$\begin{aligned} h'' + 2\mathcal{H}h' - 2\xi k^2 &= -a^2 \delta G^i_i \\ &= -8\pi G a^2 \delta T^i_i, \end{aligned} \quad (\text{C.5})$$

$$\begin{aligned}
h'' + 6\xi'' + 2\mathcal{H}(h' + 6\xi') - 2k^2\xi &= -3a^2 \left(\hat{k}_i \hat{k}_j - \frac{\delta_{ij}}{3} \right) \delta G^i{}_j \\
&= -24\pi G a^2 (\bar{\rho} + \bar{p}) \Theta
\end{aligned} \tag{C.6}$$

where we used the definition

$$(\bar{\rho} + \bar{p})\theta \equiv \iota k^i \delta T^0{}_i, \tag{C.7}$$

$$(\bar{\rho} + \bar{p})\Theta \equiv - \left(\hat{k}_i \hat{k}_j - \frac{\delta_{ij}}{3} \right) \Sigma^i{}_j, \tag{C.8}$$

$$\Sigma^i{}_j \equiv \bar{T}^i{}_j - \delta_j^i \frac{\bar{T}^k{}_k}{3}. \tag{C.9}$$

and splitting the total energy density and pressure in a background and perturbed parts, we obtain the following elements

$$\bar{T}_{00} = a^2(\bar{\rho} + \delta\rho), \tag{C.10}$$

$$\bar{T}_{0i} = -a^2(\bar{\rho} + \bar{p})v^i, \tag{C.11}$$

$$\bar{T}_{ij} = a^2\delta_{ij}(\bar{p} + \delta p) + a^2\Sigma_{ij}. \tag{C.12}$$

The first perturbed equation involving total density fluctuations reads

$$\xi k^2 - \frac{\mathcal{H}h'}{2} = -(8\pi G)a^2 \frac{\delta\tilde{\rho}}{2\bar{F}} \tag{C.13}$$

with

$$\begin{aligned}
\delta\tilde{\rho} = \delta\rho - \frac{h'\bar{\sigma}'\bar{F}_\sigma}{2a^2} + \frac{\delta\sigma'}{a^2} (Z\bar{\sigma}' - 3\mathcal{H}\bar{F}_\sigma) - \frac{\delta\sigma\bar{F}_\sigma}{a^2\bar{F}} \left[a^2\bar{\rho} + \frac{Z}{2}\bar{\sigma}'^2 \right. \\
\left. + a^2 \left(V - V_\sigma \frac{F}{F_\sigma} \right) - 3\mathcal{H}\bar{F}_\sigma\bar{\sigma}' + 3\mathcal{H} \frac{F_{\sigma\sigma}F}{F_\sigma} \bar{\sigma}' + k^2 F \right].
\end{aligned} \tag{C.14}$$

The second perturbed equation involving total velocity reads

$$k^2\xi' = (8\pi G)a^2 \frac{(\tilde{\rho} + \tilde{p})\tilde{\theta}}{2\bar{F}} \tag{C.15}$$

with

$$(\tilde{\rho} + \tilde{p})\tilde{\theta} = (\bar{\rho} + \bar{p})\theta + \frac{k^2}{a^2} [(Z\bar{\sigma}' - \mathcal{H}F_\sigma + F_{\sigma\sigma}\bar{\sigma}')\delta\sigma + F_\sigma\delta\sigma']. \tag{C.16}$$

The third perturbed equation involving total pressure reads

$$h'' + 2\mathcal{H}h' - 2k^2\xi = -3(8\pi G)a^2 \frac{\delta\tilde{p}}{F} \tag{C.17}$$

with

$$\begin{aligned}
\delta\tilde{p} = \delta p + \frac{h'F'}{3a^2} + \frac{Z}{a^2}\bar{\sigma}'\delta\sigma' - \delta V + \frac{2}{3a^2}k^2\delta F + \frac{\mathcal{H}}{a^2}\delta F' + \frac{\delta F''}{a^2} \\
- \delta\sigma \frac{\bar{F}_\sigma}{a^2\bar{F}} \left(a^2\bar{p} + \frac{Z}{2}\bar{\sigma}'^2 - a^2\bar{V} + \mathcal{H}F' + F'' \right).
\end{aligned} \tag{C.18}$$

The fourth perturbed equation involving total shear reads

$$h'' + 6\xi'' + 2\mathcal{H}(h' + 6\xi') - 2k^2\xi = -3(8\pi G)a^2\frac{(\tilde{\rho} + \tilde{p})\tilde{\Theta}}{F} \quad (\text{C.19})$$

with

$$(\tilde{\rho} + \tilde{p})\tilde{\Theta} = (\bar{\rho} + \bar{p})\Theta + \frac{2k^2}{3a^2} \left(F_\sigma \delta\sigma + F' \frac{h' + 6\xi'}{2k^2} \right). \quad (\text{C.20})$$

The perturbed Ricci scalar is given by

$$\begin{aligned} a^2 F \delta R = & a^2 (\delta\bar{\rho} - 3\delta\bar{p}) - \frac{3h'F'}{2} - 2Z\bar{\sigma}'\delta\sigma' + 4a^2 V_\sigma \delta\sigma - 6\mathcal{H}\delta F' - 3\delta F'' \\ & - 3k^2\delta F - \frac{\delta\sigma F_\sigma}{F} \left[a^2(\bar{\rho} - 3\bar{p}) - Z\bar{\sigma}'^2 + 4a^2\bar{V} - 3F'' - 6\mathcal{H}F' \right]. \end{aligned} \quad (\text{C.21})$$

C.2 The perturbed Klein-Gordon equation

The perturbed equation for the evolution of the scalar field perturbation $\delta\sigma$ is

$$Z\delta\sigma'' + 2\mathcal{H}Z\delta\sigma' + \left[Zk^2 + a^2 \left(V_{\sigma\sigma} - \frac{RF_{\sigma\sigma}}{2} \right) \right] \delta\sigma + Z\frac{h'\bar{\sigma}'}{2} - \frac{a^2 F_\sigma}{2} \delta R = 0. \quad (\text{C.22})$$

D Initial conditions

The adiabatic initial condition for the background correspond to

$$\begin{aligned} a(\tau) &= \sqrt{\frac{\rho_{r,0}}{3F_{\text{ini}}}} \tau \left[1 + \frac{Z}{4}\omega\tau - \frac{5ZF_{\text{ini},\sigma}^2(Z + 3F_{\text{ini},\sigma\sigma})}{64ZF_{\text{ini}} + 96F_{\text{ini},\sigma}^2} (\omega\tau)^2 \right], \\ \mathcal{H}(\tau) &= \frac{1}{\tau} \left[1 + \frac{Z}{4}\omega\tau - Z\frac{2F_{\text{ini}} + F_{\text{ini},\sigma}^2(8Z + 15F_{\text{ini},\sigma\sigma})}{32ZF_{\text{ini}} + 48F_{\text{ini},\sigma}^2} (\omega\tau)^2 \right], \\ \sigma(\tau) &= \sigma_{\text{ini}} + \frac{3F_{\text{ini},\sigma}}{4}\omega\tau - F_{\text{ini},\sigma} \frac{4ZF_{\text{ini}}(2Z - 3F_{\text{ini},\sigma\sigma}) + 27F_{\text{ini},\sigma}^2(Z + F_{\text{ini},\sigma\sigma})}{32(2ZF_{\text{ini}} + 3F_{\text{ini},\sigma}^2)} (\omega\tau)^2 \end{aligned} \quad (\text{D.1})$$

where

$$\omega = \frac{\rho_{m,0}}{\sqrt{3\rho_{r,0}}} \frac{2\sqrt{F_{\text{ini}}}}{2ZF_{\text{ini}} + 3F_{\text{ini},\sigma}^2}. \quad (\text{D.2})$$

For the cosmological fluctuations in the synchronous gauge, we have as adiabatic

initial conditions

$$\delta_\gamma(k, \tau) = \delta_\nu(k, \tau) = \frac{4}{3}\delta_b(k, \tau) = \frac{4}{3}\delta_c(k, \tau) = -\frac{(k\tau)^2}{3} \left(1 - \frac{Z\omega\tau}{5}\right) \quad (\text{D.3})$$

$$\theta_\nu(k, \tau) = -\frac{k^4\tau^3}{36} \frac{23 + 4R_\nu}{15 + 4R_\nu} \left[1 - \frac{3}{20} \frac{Z(275 + 50R_\nu + 8R_\nu^2)F_{\text{ini}} + 15(5 - 4R_\nu)F_{\text{ini},\sigma}^2}{(15 + 2R_\nu)(23 + 4R_\nu)F_{\text{ini}}} \omega\tau\right] \quad (\text{D.4})$$

$$\theta_\gamma(k, \tau) = \theta_b(k, \tau) = -\frac{k^4\tau^3}{36} \left[1 - \frac{3}{20} \frac{Z(1 - R_\nu + 5R_b)F_{\text{ini}} + \frac{15}{2}R_b F_{\text{ini},\sigma}^2}{(1 - R_\nu)F_{\text{ini}}} \omega\tau\right] \quad (\text{D.5})$$

$$\theta_c(k, \tau) = 0 \quad (\text{D.6})$$

$$\sigma_\nu(k, \tau) = \frac{2(k\tau)^2}{3(15 + 4R_\nu)} \left[1 + \frac{(-5 + 4R_\nu)(2ZF_{\text{ini}} + 3F_{\text{ini},\sigma}^2)}{8(15 + 2R_\nu)F_{\text{ini}}} \omega\tau\right] \quad (\text{D.7})$$

$$h(k, \tau) = \frac{(k\tau)^2}{2} \left(1 - \frac{Z\omega\tau}{5}\right) \quad (\text{D.8})$$

$$\eta(k, \tau) = 1 - \frac{(k\tau)^2}{12(15 + 4R_\nu)} \left[5 + 4R_\nu - \frac{2Z(5 + 4R_\nu)(65 + 4R_\nu)F_{\text{ini}} + 75(-5 + 4R_\nu)F_{\text{ini},\sigma}^2}{20(15 + 2R_\nu)F_{\text{ini}}} \omega\tau\right] \quad (\text{D.9})$$

$$\delta\sigma(k, \tau) = -\frac{1}{16}F_{\text{ini},\sigma}k^2\tau^3\omega \left[1 - \frac{2Z(8Z - 9F_{\text{ini},\sigma\sigma})F_{\text{ini}} + (45F_{\text{ini},\sigma\sigma} + 48Z)F_{\text{ini},\sigma}^2}{40ZF_{\text{ini}} + 60F_{\text{ini},\sigma}^2} \omega\tau\right] \quad (\text{D.10})$$

where $R_\nu = \rho_{\nu,0}/\rho_{r,0}$ and $R_b = \rho_{b,0}/\rho_{m,0}$. These quantities reduce to induced gravity for $Z = 1$ and $F = \xi\sigma^2$ [89], to a non-minimally coupled scalar field with standard kinetic term for $Z = 1$ and $F = N_{\text{Pl}}^2 + \xi\sigma^2$ [14], and General Relativity for $Z = 1$ and $F = M_{\text{Pl}}^2$ [88].

E Comparison between BAO, and FS + BAO joint analysis

We compare here the results adding different datasets of galaxy information to the *Planck* DR3 data such as the full shape (FS) of BOSS DR12 pre-reconstructed power spectrum measurements [66, 67], BAO of BOSS DR12 post-reconstruction power spectrum measurements [68], low- z BAO measurements from SDSS DR7 6dF and MGS [69, 70], Ly α BAO measurements from eBOSS [71–73], and combination of those including the covariance among the DR12 datasets.

In Fig. 11, we show the marginalized posterior distributions of the cosmological parameters for IG with P18 plus different combinations of the FS and BAO measurements. We see that the posterior distributions are very robust among the combination considered and that the addition of FS information to the combination P18+BAO does not change the marginalized constraints for the models studied here.

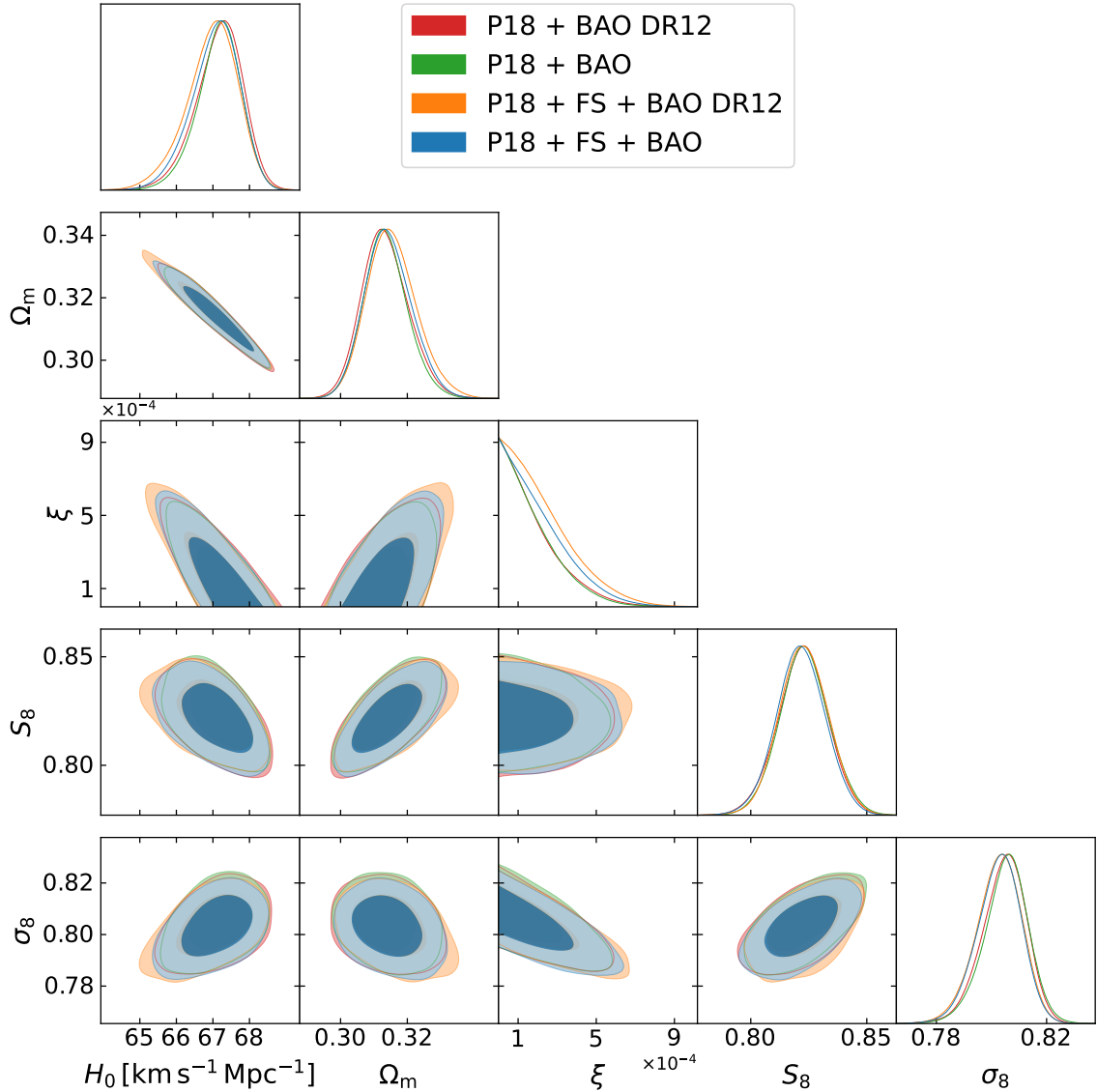


Figure 11. Marginalized joint 68% and 95% CL regions 2D parameter space using the CMB P18 data for IG ($F = \xi\sigma^2$) in the phantom branch ($Z = -1$) in combination with BAO from BOSS DR12 (red), BAO from BOSS DR12/SDSS DR7 6dF-MGS/eBOSS (green), FS plus BAO from BOSS DR12 (orange), and FS plus BAO from BOSS DR12/SDSS DR7 6dF-MGS/eBOSS (blue).

References

- [1] Adam G. Riess et al. Observational evidence from supernovae for an accelerating universe and a cosmological constant. *Astron. J.*, 116:1009–1038, 1998. doi: 10.1086/300499.
- [2] S. Perlmutter et al. Measurements of Ω and Λ from 42 high redshift supernovae. *Astrophys. J.*, 517:565–586, 1999. doi: 10.1086/307221.

- [3] Anthony Carr, Tamara M. Davis, Daniel Scolnic, Khaled Said, Dillon Brout, Erik R. Peterson, and Richard Kessler. The Pantheon+ Analysis: Improving the Redshifts and Peculiar Velocities of Type Ia Supernovae Used in Cosmological Analyses. 12 2021.
- [4] N. Aghanim et al. Planck 2018 results. I. Overview and the cosmological legacy of Planck. *Astron. Astrophys.*, 641:A1, 2020. doi: 10.1051/0004-6361/201833880.
- [5] Shadab Alam et al. Completed SDSS-IV extended Baryon Oscillation Spectroscopic Survey: Cosmological implications from two decades of spectroscopic surveys at the Apache Point Observatory. *Phys. Rev. D*, 103(8):083533, 2021. doi: 10.1103/PhysRevD.103.083533.
- [6] A. Veropalumbo, F. Marulli, L. Moscardini, M. Moresco, and A. Cimatti. An improved measurement of baryon acoustic oscillations from the correlation function of galaxy clusters at $z \sim 0.3$. *Mon. Not. Roy. Astron. Soc.*, 442(4):3275–3283, 2014. doi: 10.1093/mnras/stu1050.
- [7] Blake D. Sherwin et al. Two-season Atacama Cosmology Telescope polarimeter lensing power spectrum. *Phys. Rev. D*, 95(12):123529, 2017. doi: 10.1103/PhysRevD.95.123529.
- [8] W. L. K. Wu et al. A Measurement of the Cosmic Microwave Background Lensing Potential and Power Spectrum from 500 deg² of SPTpol Temperature and Polarization Data. *Astrophys. J.*, 884:70, 2019. doi: 10.3847/1538-4357/ab4186.
- [9] Omar Darwish et al. The Atacama Cosmology Telescope: A CMB lensing mass map over 2100 square degrees of sky and its cross-correlation with BOSS-CMASS galaxies. *Mon. Not. Roy. Astron. Soc.*, 500(2):2250–2263, 2020. doi: 10.1093/mnras/staa3438.
- [10] Marika Asgari et al. KiDS-1000 Cosmology: Cosmic shear constraints and comparison between two point statistics. *Astron. Astrophys.*, 645:A104, 2021. doi: 10.1051/0004-6361/202039070.
- [11] T. M. C. Abbott et al. Dark Energy Survey Year 3 results: Cosmological constraints from galaxy clustering and weak lensing. *Phys. Rev. D*, 105(2):023520, 2022. doi: 10.1103/PhysRevD.105.023520.
- [12] Ryan J. Cooke, Max Pettini, and Charles C. Steidel. One Percent Determination of the Primordial Deuterium Abundance. *Astrophys. J.*, 855(2):102, 2018. doi: 10.3847/1538-4357/aaab53.
- [13] C. Umiltà, M. Ballardini, F. Finelli, and D. Paoletti. CMB and BAO constraints for an induced gravity dark energy model with a quartic potential. *JCAP*, 08:017, 2015. doi: 10.1088/1475-7516/2015/08/017.
- [14] Massimo Rossi, Mario Ballardini, Matteo Braglia, Fabio Finelli, Daniela Paoletti, Alexei A. Starobinsky, and Caterina Umiltà. Cosmological constraints on post-Newtonian parameters in effectively massless scalar-tensor theories of gravity. *Phys. Rev. D*, 100(10):103524, 2019. doi: 10.1103/PhysRevD.100.103524.
- [15] Vivian Poulin, Tristan L. Smith, Tanvi Karwal, and Marc Kamionkowski. Early Dark Energy Can Resolve The Hubble Tension. *Phys. Rev. Lett.*, 122(22):221301, 2019. doi: 10.1103/PhysRevLett.122.221301.

- [16] Prateek Agrawal, Francis-Yan Cyr-Racine, David Pinner, and Lisa Randall. Rock ‘n’ Roll Solutions to the Hubble Tension. 4 2019. arXiv: 1904.01016.
- [17] Luke Hart and Jens Chluba. Updated fundamental constant constraints from Planck 2018 data and possible relations to the Hubble tension. *Mon. Not. Roy. Astron. Soc.*, 493(3):3255–3263, 2020. doi: 10.1093/mnras/staa412.
- [18] Karsten Jedamzik and Levon Pogosian. Relieving the Hubble tension with primordial magnetic fields. *Phys. Rev. Lett.*, 125(18):181302, 2020. doi: 10.1103/PhysRevLett.125.181302.
- [19] Mario Ballardini, Matteo Braglia, Fabio Finelli, Daniela Paoletti, Alexei A. Starobinsky, and Caterina Umiltà. Scalar-tensor theories of gravity, neutrino physics, and the H_0 tension. *JCAP*, 10:044, 2020. doi: 10.1088/1475-7516/2020/10/044.
- [20] Matteo Braglia, Mario Ballardini, Fabio Finelli, and Kazuya Koyama. Early modified gravity in light of the H_0 tension and LSS data. *Phys. Rev. D*, 103(4):043528, 2021. doi: 10.1103/PhysRevD.103.043528.
- [21] Akhil Antony, Fabio Finelli, Dhiraj Kumar Hazra, and Arman Shafieloo. Discordances in cosmology and the violation of slow-roll inflationary dynamics. 2022.
- [22] Lloyd Knox and Marius Millea. Hubble constant hunter’s guide. *Phys. Rev. D*, 101(4):043533, 2020. doi: 10.1103/PhysRevD.101.043533.
- [23] Eleonora Di Valentino et al. Snowmass2021 - Letter of interest cosmology intertwined II: The hubble constant tension. *Astropart. Phys.*, 131:102605, 2021. doi: 10.1016/j.astropartphys.2021.102605.
- [24] Eleonora Di Valentino et al. Cosmology intertwined III: $f\sigma_8$ and S_8 . *Astropart. Phys.*, 131:102604, 2021. doi: 10.1016/j.astropartphys.2021.102604.
- [25] Eleonora Di Valentino, Olga Mena, Supriya Pan, Luca Visinelli, Weiqiang Yang, Alessandro Melchiorri, David F. Mota, Adam G. Riess, and Joseph Silk. In the realm of the Hubble tension—a review of solutions. *Class. Quant. Grav.*, 38(15):153001, 2021. doi: 10.1088/1361-6382/ac086d.
- [26] Leandros Perivolaropoulos and Foteini Skara. Challenges for Λ CDM: An update. *New Astron. Rev.*, 95, 2022. doi: 10.1016/j.newar.2022.101659.
- [27] Nils Schöneberg, Guillermo Franco Abellán, Andrea Pérez Sánchez, Samuel J. Witte, Vivian Poulin, and Julien Lesgourgues. The H_0 Olympics: A fair ranking of proposed models. 7 2021. arXiv: 2107.10291.
- [28] Paul Shah, Pablo Lemos, and Ofer Lahav. A buyer’s guide to the Hubble constant. *Astron. Astrophys. Rev.*, 29(1):9, 2021. doi: 10.1007/s00159-021-00137-4.
- [29] Elcio Abdalla et al. Cosmology intertwined: A review of the particle physics, astrophysics, and cosmology associated with the cosmological tensions and anomalies. *JHEAp*, 34:49–211, 2022. doi: 10.1016/j.jheap.2022.04.002.
- [30] N. Aghanim et al. Planck 2018 results. VI. Cosmological parameters. *Astron. Astrophys.*, 641:A6, 2020. doi: 10.1051/0004-6361/201833910. [Erratum: *Astron. Astrophys.* 652, C4 (2021)].
- [31] Adam G. Riess et al. A Comprehensive Measurement of the Local Value of the Hubble

- Constant with $1 \text{ km s}^{-1} \text{ Mpc}^{-1}$ Uncertainty from the Hubble Space Telescope and the SHOES Team. *Astrophys. J. Lett.*, 934(1):L7, 2022. doi: 10.3847/2041-8213/ac5c5b.
- [32] Mario Ballardini, Fabio Finelli, Caterina Umiltà, and Daniela Paoletti. Cosmological constraints on induced gravity dark energy models. *JCAP*, 05:067, 2016. doi: 10.1088/1475-7516/2016/05/067.
- [33] J. Colin Hill, Evan McDonough, Michael W. Toomey, and Stephon Alexander. Early dark energy does not restore cosmological concordance. *Phys. Rev. D*, 102(4):043507, 2020. doi: 10.1103/PhysRevD.102.043507.
- [34] Matteo Braglia, Mario Ballardini, William T. Emond, Fabio Finelli, A. Emir Gumrukcuoglu, Kazuya Koyama, and Daniela Paoletti. Larger value for H_0 by an evolving gravitational constant. *Phys. Rev. D*, 102(2):023529, 2020. doi: 10.1103/PhysRevD.102.023529.
- [35] Mikhail M. Ivanov, Evan McDonough, J. Colin Hill, Marko Simonović, Michael W. Toomey, Stephon Alexander, and Matias Zaldarriaga. Constraining Early Dark Energy with Large-Scale Structure. *Phys. Rev. D*, 102(10):103502, 2020. doi: 10.1103/PhysRevD.102.103502.
- [36] K. Rezazadeh, A. Ashoorioon, and D. Grin. Cascading Dark Energy. 8 2022.
- [37] Tristan L. Smith, Vivian Poulin, José Luis Bernal, Kimberly K. Boddy, Marc Kamionkowski, and Riccardo Murgia. Early dark energy is not excluded by current large-scale structure data. *Phys. Rev. D*, 103(12):123542, 2021. doi: 10.1103/PhysRevD.103.123542.
- [38] Mario Ballardini, Fabio Finelli, and Domenico Sapone. Cosmological constraints on the gravitational constant. *JCAP*, 06(06):004, 2022. doi: 10.1088/1475-7516/2022/06/004.
- [39] Théo Simon, Pierre Zhang, Vivian Poulin, and Tristan L. Smith. Updated constraints from the effective field theory analysis of BOSS power spectrum on Early Dark Energy. 8 2022. arXiv: 2208.05930.
- [40] Evan McDonough, Meng-Xiang Lin, J. Colin Hill, Wayne Hu, and Shengjia Zhou. Early dark sector, the Hubble tension, and the swampland. *Phys. Rev. D*, 106(4):043525, 2022. doi: 10.1103/PhysRevD.106.043525.
- [41] Adrià Gómez-Valent, Ziyang Zheng, Luca Amendola, Christof Wetterich, and Valeria Pettorino. Coupled and uncoupled early dark energy, massive neutrinos and the cosmological tensions. 7 2022. arXiv: 2207.14487.
- [42] Alexander Reeves, Laura Herold, Sunny Vagnozzi, Blake D. Sherwin, and Elisa G. M. Ferreira. Restoring cosmological concordance with early dark energy and massive neutrinos? 7 2022. arXiv: 2207.01501.
- [43] B. Boisseau, Gilles Esposito-Farese, D. Polarski, and Alexei A. Starobinsky. Reconstruction of a scalar tensor theory of gravity in an accelerating universe. *Phys. Rev. Lett.*, 85:2236, 2000. doi: 10.1103/PhysRevLett.85.2236.
- [44] R. R. Caldwell. A Phantom menace? *Phys. Lett. B*, 545:23–29, 2002. doi: 10.1016/S0370-2693(02)02589-3.
- [45] James M. Cline, Sangyong Jeon, and Guy D. Moore. The Phantom menaced:

- Constraints on low-energy effective ghosts. *Phys. Rev. D*, 70:043543, 2004. doi: 10.1103/PhysRevD.70.043543.
- [46] Hans Peter Nilles. Supersymmetry, Supergravity and Particle Physics. *Phys. Rept.*, 110:1–162, 1984. doi: 10.1016/0370-1573(84)90008-5.
- [47] M. D. Pollock. On the Initial Conditions for Superexponential Inflation. *Phys. Lett. B*, 215:635–641, 1988. doi: 10.1016/0370-2693(88)90034-2.
- [48] Radouane Gannouji, David Polarski, Andre Ranquet, and Alexei A. Starobinsky. Scalar-Tensor Models of Normal and Phantom Dark Energy. *JCAP*, 09:016, 2006. doi: 10.1088/1475-7516/2006/09/016.
- [49] B. Bertotti, L. Iess, and P. Tortora. A test of general relativity using radio links with the Cassini spacecraft. *Nature*, 425:374–376, 2003. doi: 10.1038/nature01997.
- [50] Timothy Clifton, John D. Barrow, and Robert J. Scherrer. Constraints on the variation of G from primordial nucleosynthesis. *Phys. Rev. D*, 71:123526, 2005. doi: 10.1103/PhysRevD.71.123526.
- [51] Jurgen Muller and Liliane Biskupek. Variations of the gravitational constant from lunar laser ranging data. *Class. Quant. Grav.*, 24:4533–4538, 2007. doi: 10.1088/0264-9381/24/17/017.
- [52] Enis Belgacem, Andreas Finke, Antonia Frassino, and Michele Maggiore. Testing nonlocal gravity with Lunar Laser Ranging. *JCAP*, 02:035, 2019. doi: 10.1088/1475-7516/2019/02/035.
- [53] David Alonso, Emilio Bellini, Pedro G. Ferreira, and Miguel Zumalacárregui. Observational future of cosmological scalar-tensor theories. *Phys. Rev. D*, 95(6): 063502, 2017. doi: 10.1103/PhysRevD.95.063502.
- [54] M. Ballardini, D. Sapone, C. Umiltà, F. Finelli, and D. Paoletti. Testing extended Jordan-Brans-Dicke theories with future cosmological observations. *JCAP*, 05:049, 2019. doi: 10.1088/1475-7516/2019/05/049.
- [55] Gilles Esposito-Farese and D. Polarski. Scalar tensor gravity in an accelerating universe. *Phys. Rev. D*, 63:063504, 2001. doi: 10.1103/PhysRevD.63.063504.
- [56] Fred Cooper and Giovanni Venturi. Cosmology and Broken Scale Invariance. *Phys. Rev. D*, 24:3338, 1981. doi: 10.1103/PhysRevD.24.3338.
- [57] C. Wetterich. Cosmologies With Variable Newton’s ‘Constant’. *Nucl. Phys. B*, 302: 645–667, 1988. doi: 10.1016/0550-3213(88)90192-7.
- [58] Luca Amendola. Scaling solutions in general nonminimal coupling theories. *Phys. Rev. D*, 60:043501, 1999. doi: 10.1103/PhysRevD.60.043501.
- [59] F. Finelli, A. Tronconi, and Giovanni Venturi. Dark Energy, Induced Gravity and Broken Scale Invariance. *Phys. Lett. B*, 659:466–470, 2008. doi: 10.1016/j.physletb.2007.11.053.
- [60] Julien Lesgourgues. The Cosmic Linear Anisotropy Solving System (CLASS) I: Overview. 4 2011. arXiv: 1104.2932.
- [61] Diego Blas, Julien Lesgourgues, and Thomas Tram. The Cosmic Linear Anisotropy

- Solving System (CLASS) II: Approximation schemes. *JCAP*, 07:034, 2011. doi: 10.1088/1475-7516/2011/07/034.
- [62] Benjamin Audren, Julien Lesgourgues, Karim Benabed, and Simon Prunet. Conservative Constraints on Early Cosmology: an illustration of the Monte Python cosmological parameter inference code. *JCAP*, 02:001, 2013. doi: 10.1088/1475-7516/2013/02/001.
- [63] Thejs Brinckmann and Julien Lesgourgues. MontePython 3: boosted MCMC sampler and other features. *Phys. Dark Univ.*, 24:100260, 2019. doi: 10.1016/j.dark.2018.100260.
- [64] N. Aghanim et al. Planck 2018 results. V. CMB power spectra and likelihoods. *Astron. Astrophys.*, 641:A5, 2020. doi: 10.1051/0004-6361/201936386.
- [65] N. Aghanim et al. Planck 2018 results. VIII. Gravitational lensing. *Astron. Astrophys.*, 641:A8, 2020. doi: 10.1051/0004-6361/201833886.
- [66] Héctor Gil-Marín et al. The clustering of galaxies in the SDSS-III Baryon Oscillation Spectroscopic Survey: RSD measurement from the LOS-dependent power spectrum of DR12 BOSS galaxies. *Mon. Not. Roy. Astron. Soc.*, 460(4):4188–4209, 2016. doi: 10.1093/mnras/stw1096.
- [67] Guido D’Amico, Leonardo Senatore, and Pierre Zhang. Limits on w CDM from the EFTofLSS with the PyBird code. *JCAP*, 01:006, 2021. doi: 10.1088/1475-7516/2021/01/006.
- [68] Shadab Alam et al. The clustering of galaxies in the completed SDSS-III Baryon Oscillation Spectroscopic Survey: cosmological analysis of the DR12 galaxy sample. *Mon. Not. Roy. Astron. Soc.*, 470(3):2617–2652, 2017. doi: 10.1093/mnras/stx721.
- [69] Florian Beutler, Chris Blake, Matthew Colless, D. Heath Jones, Lister Staveley-Smith, Lachlan Campbell, Quentin Parker, Will Saunders, and Fred Watson. The 6dF Galaxy Survey: Baryon Acoustic Oscillations and the Local Hubble Constant. *Mon. Not. Roy. Astron. Soc.*, 416:3017–3032, 2011. doi: 10.1111/j.1365-2966.2011.19250.x.
- [70] Ashley J. Ross, Lado Samushia, Cullan Howlett, Will J. Percival, Angela Burden, and Marc Manera. The clustering of the SDSS DR7 main Galaxy sample – I. A 4 per cent distance measure at $z = 0.15$. *Mon. Not. Roy. Astron. Soc.*, 449(1):835–847, 2015. doi: 10.1093/mnras/stv154.
- [71] Victoria de Sainte Agathe et al. Baryon acoustic oscillations at $z = 2.34$ from the correlations of $\text{Ly}\alpha$ absorption in eBOSS DR14. *Astron. Astrophys.*, 629:A85, 2019. doi: 10.1051/0004-6361/201935638.
- [72] Michael Blomqvist et al. Baryon acoustic oscillations from the cross-correlation of $\text{Ly}\alpha$ absorption and quasars in eBOSS DR14. *Astron. Astrophys.*, 629:A86, 2019. doi: 10.1051/0004-6361/201935641.
- [73] Andrei Cuceu, James Farr, Pablo Lemos, and Andreu Font-Ribera. Baryon Acoustic Oscillations and the Hubble Constant: Past, Present and Future. *JCAP*, 10:044, 2019. doi: 10.1088/1475-7516/2019/10/044.
- [74] D. M. Scolnic et al. The Complete Light-curve Sample of Spectroscopically Confirmed

- SNe Ia from Pan-STARRS1 and Cosmological Constraints from the Combined Pantheon Sample. *Astrophys. J.*, 859(2):101, 2018. doi: 10.3847/1538-4357/aab9bb.
- [75] O. Pisanti, A. Cirillo, S. Esposito, F. Iocco, G. Mangano, G. Miele, and P. D. Serpico. PArthENoPE: Public Algorithm Evaluating the Nucleosynthesis of Primordial Elements. *Comput. Phys. Commun.*, 178:956–971, 2008. doi: 10.1016/j.cpc.2008.02.015.
- [76] R. Consiglio, P. F. de Salas, G. Mangano, G. Miele, S. Pastor, and O. Pisanti. PArthENoPE reloaded. *Comput. Phys. Commun.*, 233:237–242, 2018. doi: 10.1016/j.cpc.2018.06.022.
- [77] Miguel Zumalacarregui. Gravity in the Era of Equality: Towards solutions to the Hubble problem without fine-tuned initial conditions. *Phys. Rev. D*, 102(2):023523, 2020. doi: 10.1103/PhysRevD.102.023523.
- [78] Joan Solà Peracaula, Adrià Gómez-Valent, Javier de Cruz Pérez, and Cristian Moreno-Pulido. Brans–Dicke cosmology with a Λ -term: a possible solution to Λ CDM tensions. *Class. Quant. Grav.*, 37(24):245003, 2020. doi: 10.1088/1361-6382/abbc43.
- [79] Mario Ballardini and Fabio Finelli. Type Ia supernovae data with scalar-tensor gravity. *Phys. Rev. D*, 106(6):063531, 2022. doi: 10.1103/PhysRevD.106.063531.
- [80] Jaume Garriga and Viatcheslav F. Mukhanov. Perturbations in k-inflation. *Phys. Lett. B*, 458:219–225, 1999. doi: 10.1016/S0370-2693(99)00602-4.
- [81] M. Gasperini and G. Veneziano. The Pre - big bang scenario in string cosmology. *Phys. Rept.*, 373:1–212, 2003. doi: 10.1016/S0370-1573(02)00389-7.
- [82] Nima Arkani-Hamed, Hsin-Chia Cheng, Markus A. Luty, and Shinji Mukohyama. Ghost condensation and a consistent infrared modification of gravity. *JHEP*, 05:074, 2004. doi: 10.1088/1126-6708/2004/05/074.
- [83] Alberto Nicolis, Riccardo Rattazzi, and Enrico Trincherini. The Galileon as a local modification of gravity. *Phys. Rev. D*, 79:064036, 2009. doi: 10.1103/PhysRevD.79.064036.
- [84] C. Deffayet, Gilles Esposito-Farese, and A. Vikman. Covariant Galileon. *Phys. Rev. D*, 79:084003, 2009. doi: 10.1103/PhysRevD.79.084003.
- [85] Fabio P Silva and Kazuya Koyama. Self-Accelerating Universe in Galileon Cosmology. *Phys. Rev. D*, 80:121301, 2009. doi: 10.1103/PhysRevD.80.121301.
- [86] Tsutomu Kobayashi. Cosmic expansion and growth histories in Galileon scalar-tensor models of dark energy. *Phys. Rev. D*, 81:103533, 2010. doi: 10.1103/PhysRevD.81.103533.
- [87] Angelo Ferrari and et al. in preparation (2023).
- [88] Chung-Pei Ma and Edmund Bertschinger. Cosmological perturbation theory in the synchronous and conformal Newtonian gauges. *Astrophys. J.*, 455:7–25, 1995. doi: 10.1086/176550.
- [89] D. Paoletti, M. Braglia, F. Finelli, M. Ballardini, and C. Umiltà. Isocurvature fluctuations in the effective Newton’s constant. *Phys. Dark Univ.*, 25:100307, 2019. doi: 10.1016/j.dark.2019.100307.